minerals

MDPI

Article

Provenance of the Upper Paleozoic Shihezi Formation in the Luonan Region of the Qinling Orogenic Belt and Its Tectonic Implications

Yuliang Duan [1,2], Wenqi Pan [3,*], Xi Zhang [4], Zhengtao Zhang [5,6], Yi Ding [7,*], Ziwen Jiang [3], Zhichao Li [5,6], Lamao Meiduo [3], Weiran Zhao [3] and Wenhou Li [1]

1 State Key Laboratory of Continental Dynamics, Department of Geology, Northwest University, Xi'an 710069, China; yuliangduan211@gmail.com (Y.D.); liwenhou@nwu.edu.cn (W.L.)
2 Yanchang Oilfield Co., Ltd., Yan'an 716000, China
3 Key Lab of Cenozoic Resource and Environment in North Margin of the Tibetan Plateau, School of Geological Engineering, Qinghai University, Xining 810016, China; jiangziwen0601@163.com (Z.J.); 16601119625@163.com (L.M.); zhaoweiran200103@163.com (W.Z.)
4 Oilfield Development Department, PetroChina Changqing Oilfield Co., Ltd., Xi'an 710018, China; zxi_cq@petrochina.com.cn
5 National Engineering Laboratory of Low Permeability Oil and Gas Field Exploration and Development, PetroChina Changqing Oilfield Co., Ltd., Xi'an 710018, China; zhangzt_cq@petrochina.com.cn (Z.Z.); lzc3_cq@petrochina.com.cn (Z.L.)
6 Research Institute of Petroleum Exploration and Development, PetroChina Changqing Oilfield Co., Ltd., Xi'an 710018, China
7 College of Environment and Life Science, Weinan Normal University, Weinan 714099, China
* Correspondence: panwenqi0421@163.com (W.P.); dingyi@nwu.edu.cn (Y.D.)

Abstract: This study investigates the provenance of the Permian Shihezi Formation (Fm) siliciclastic sediments in the Luonan area, southern margin of the North China Block, which constrain the sediment sources and tectonic evolution of the basin. Our research investigates the heavy mineral characteristics, geochemical features, detrital zircon U-Pb geochronology, and Lu-Hf isotope tracing the provenance characteristics of the Shihezi Fm in this region. Zircon yielded three distinct U-Pb age groups as follows: 320–300 Ma, 1950–1850 Ma, and 2550–2450 Ma. The $\varepsilon_{Hf}(t)$ values of zircons ranged from −41 to 50, and the two–stage Hf model's ages (T_{DM2}) values are concentrated between 3940 Ma and 409 Ma, suggesting that magmatic sources likely derive from Early Archaean–Devonian crustal materials. The heavy mineral assemblages are primarily composed of zircon, leucoxene, and magnetite. Further geochemical analyses of the rocks indicate a diverse provenance area and a complex tectonic evolution. Taken together, these results suggest that the provenance of the Shihezi Fm is from the North China Block, with secondary contributions from the Qinling Orogenic Belt and the North Qilian Orogenic Belt. The provenance of Luonan shares similarities with the southern Ordos Basin. Investigating the provenance of the Luonan area along the southern margin of the North China Craton provides critical supplementary constraints for shedding light on the Late Paleozoic tectonothermal events in the Qinling Orogenic Belt.

Keywords: provenance; detrital zircon; heavy mineral; U-Pb dating; in situ Lu-Hf isotope; Luonan

check for updates

Academic Editor: Ilya Bindeman

Received: 8 April 2025
Revised: 7 May 2025
Accepted: 17 May 2025
Published: 21 May 2025

Citation: Duan, Y.; Pan, W.; Zhang, X.; Zhang, Z.; Ding, Y.; Jiang, Z.; Li, Z.; Meiduo, L.; Zhao, W.; Li, W. Provenance of the Upper Paleozoic Shihezi Formation in the Luonan Region of the Qinling Orogenic Belt and Its Tectonic Implications. *Minerals* **2025**, *15*, 549. https://doi.org/10.3390/min15050549

Copyright: © 2025 by the authors. Licensee MDPI, Basel, Switzerland. This article is an open access article distributed under the terms and conditions of the Creative Commons Attribution (CC BY) license (https://creativecommons.org/licenses/by/4.0/).

1. Introduction

The collisional architecture of the Qinling Orogenic Belt during the Paleozoic–Mesozoic was governed by convergent tectonics among the North China Craton, Yangtze Craton,

and Qinling Terrane [1,2]. From the north to the south, the geological framework consists of the southern margin of the North China Block, characterized by Paleozoic accretionary strata, followed by the North Qinling Orogenic Belt (NQinOB) and the South Qinling Orogenic Belt (SQinOB), which was primarily shaped by collisions during the early to middle Mesozoic, along with the northern margin of the Yangtze Block (Figure 1) [3,4]. The study area is located in Luonan County, Shaanxi Province, China, with a tectonic position on the southern margin of the North China Block [5]. It lies north of the Luonan–Luanchuan Fault Zone (Figure 1). A few researchers have studied provenance using methods such as paleo-flow analysis [6], sedimentological and petrological approaches [7], geochemical characteristics [6], and detrital zircon analysis [6,7]. Notably, Professor Yang Wentao's research team has conducted systematic provenance analyses in this region [7]. However, recent research findings indicate a discrepancy with his provenance results. Therefore, further investigation is necessary. This has led to an unclear understanding of the provenance of the Luonan strata. Luonan, situated north of the Luonan–Luanchuan Fault, contains the Shihezi Formation (Fm), and it is the only Permian formation in this area that provides evidence that the provenance in Luonan can constrain the tectonic evolution of both the North China Block and NQinOB [8]. Focusing on the southern margin of the North China Block, this research targets the Middle Permian Shihezi Formation in the Luonan area. It employs heavy mineral analysis, sedimentary geochemistry, detrital zircon U-Pb dating, and Lu-Hf isotope tracing methods to investigate the provenance of sediments.

2. Geological Background

Luonan lies to the north of NQinOB (Figure 1a), while the Ordos Basin lies to the north of the Luonan–Luanchuan Fault Zone (Figure 1b). The two regions are geographically adjacent, with the Ordos Basin forming the northern boundary and Luonan positioned to the south. During the Late Early Paleozoic (440–420 Ma), the closure of the North Qinling Ocean resulted in a collision between the North China Block and the Qinling terrane. The uplift associated with this phase provided recycled orogenic materials to the Middle Permian Shihezi Fm in the Luonan area along the southern margin of the North China Block [9]. From the Carboniferous to Permian, tectonic activity along the Shangdan Fault Zone between the North China Block and the Yangtze Block induced rifting processes, resulting in the formation of an intermontane rift basin in the Luonan region. The Shihezi Fm was deposited in this extensional environment [10]. By the Middle Permian, a collision between the North China Block and the Qinling terrane resulted in the rapid exhumation of NQinOB, accompanied by diminished sediment supply from South Qinling. Consequently, the provenance of the Shihezi Fm shifted to dominantly intermediate–felsic igneous rocks, low-grade metamorphic rocks, and sedimentary rocks derived from the NQinOB, reflecting stage-specific variations in tectonic dynamics [11,12]. The stratigraphy of the Luonan area mainly includes Precambrian–Mesozoic units.

The Shihezi Formation (Luonan area), situated along the southern edge of the North China Block, exhibits tectonic continuity with the Ordos Basin's southern periphery. Specimens obtained in the Hancheng region, a key sector of the Ordos Basin's southeast cratonic margin, were also collected in this research to conduct a comparative study with the Luonan region for integrated analysis and systematic comparison. Due to tectonic uplift, the Shihezi Formation in the study area is thinly exposed. Its lithology comprises the following: Lower section: rhythmically interbedded gray-black and variegated silty mudstone, mudstone, gray-white–gray-black sandstone, and a conglomerate of varying thicknesses, with coal seams. Upper section: gray-white fine sandstone, gray-black–gray-white silty mudstone, and clayey mudstone. Hancheng: yellowish-green sandstone collected west of Provincial

Highway S304, Zhuyuan Village, Hancheng City. Luonan (LN-03, LN-20): gray-white medium sandstone collected at the 21.9 km mark of Provincial Highway S307, Yaochuan Village, Yaoxi Town, Luonan County.

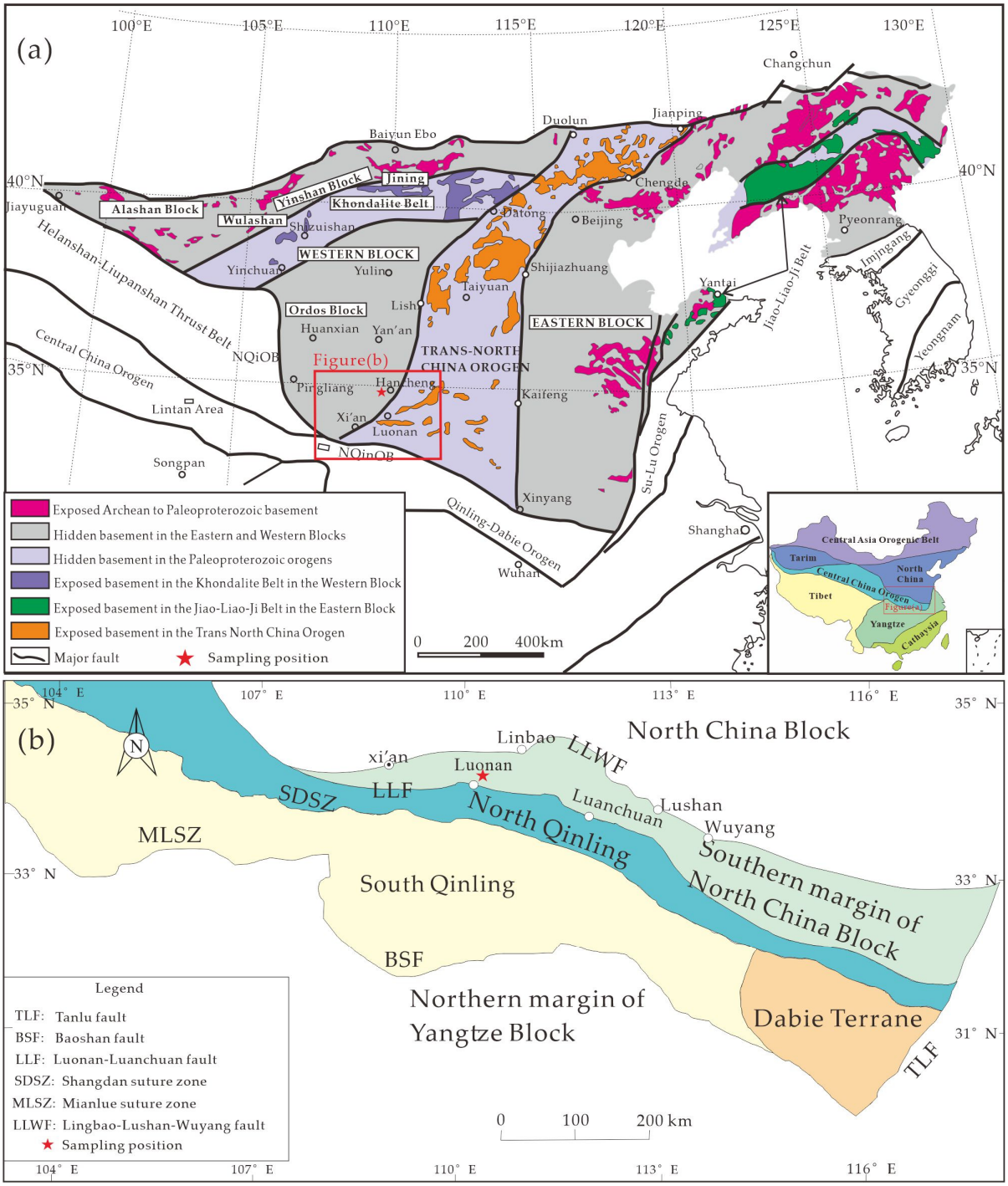


Figure 1. Tectonic location of the study area ((**a**) modified from [13]; (**b**) modified from [14,15]; plotted with CorelDRAW Graphics Suite 2021 software, version 23.5.0.506).

3. Sampling and Methodology

3.1. Heavy Minerals Analysis

Heavy mineral characteristic analyses were performed on the sandstone samples HC-01 (Hancheng), HC-12 (Hancheng), LN-03 (Luonan), LN-12 (Luonan), and LN-20 (Luonan). The sample preparation and heavy liquid separation methods follow those

described by Morton and Hallsworth [16]. The specific steps are as follows: After crushing the samples, they were sieved and washed. Subsequently, the samples were repeatedly magnetically separated using an electromagnet until the strongly magnetic minerals were completely removed, thereby increasing purity. The samples were then further refined by fine washing, and finally, the heavy mineral species were identified under a binocular microscope. The aforementioned separation and identification of heavy minerals were performed by the Hebei Provincial Institute of Regional Geological Survey.

3.2. Sedimentary Geochemistry Analysis

Twenty-one sandstone samples were used for primary trace element analytical testing in the research area. Samples HC-01 (Hancheng), HC-03 (Hancheng), HC-05 (Hancheng), HC-08 (Hancheng), HC-10 (Hancheng), HC-11 (Hancheng), HC-14 (Hancheng), HC-16 (Hancheng), HC-17 (Hancheng), HC-19 (Hancheng), and HC-20 (Hancheng) were collected and tested in the Hancheng area, while samples LN-05 (Luonan), LN-06 (Luonan), LN-07 (Luonan), LN-08 (Luonan), LN-10 (Luonan), LN-17 (Luonan), LN-23 (Luonan), LN-25 (Luonan), LN-27 (Luonan), and LN-28 (Luonan) were in the Luonan area.

The major and trace elements were analyzed at the State Key Laboratory of Continental Dynamics, Northwest University, China. Based on the characteristics of the field rock masses, hand specimens, and microscopic observations, the major element compositions of 21 whole-rock samples were determined via wavelength-dispersive X-ray fluorescence spectrometry on a Rigaku XRF-2100 (RIX2100, ZSXPrimusII, RIGAKU Corporation, Tokyo, Japan) system, with fused glass beads prepared following standard procedures. The trace element analysis of the entire rock was performed using an Elan 6100 DC (Perkin Elmer Elan 6100DC, Shelton, CT, USA) inductively coupled plasma mass spectrometer (ICP-MS). During the testing process, one quality control (QC) standard sample was analyzed for every ten samples. Each batch of solution analyses included two BHVO-2 standards, two AGV-2 standards, and one BCR-2 standard material. The analysis precision for elements, such as Y, Zr, Nb, Co, Ni, Rb, Hf, Ta, Zn, and Ga, and rare earth elements (REEs), except for Hf and Lu, was better than 5%. Meanwhile, the precision for other low-concentration elements ranged from 5% to 10% [17]. A detailed analysis of the testing process can be found in [18]. The results are listed in Tables S1 and S2 in the Supplementary Materials.

3.3. LA-ICP-MS Zircon Dating and Zircon Lu-Hf Isotopic Analysis

Coupled U-Pb and Lu-Hf isotopic studies were performed on the following three sandstone-hosted detrital zircon populations: HC-01 (Hancheng), LN-03 (Luonan), and LN-20 (Luonan).

The samples were initially observed in the field, followed by separation, which was carried out in the laboratory of the Hebei Regional Geological Survey Team. The zircon separation procedure for the studied rock samples included the following steps: washing, oven-drying, crushing to 50–80 mesh, gravity separation, magnetic separation, heavy liquid separation, and the final selection of zircon grains under a binocular microscope. First, zircon grains that are inclusion-free, highly transparent, and crack-free were randomly selected under a stereomicroscope. The zircon grains were fixed with colorless transparent epoxy resin on double-sided tape, and they were then polished to expose the zircon center. Microscopic photography of the zircon crystals was performed, with transmitted and reflected light images showing surface and internal fractures and inclusions. These images aid in selecting zircon grains and point locations. Cathodoluminescence (CL) images reveal the internal structure of the zircons.

The zircon dating and in situ analysis of Lu-Hf isotopes were conducted at the State Key Laboratory of Continental Dynamics, Northwest University, China. Zircon U-Pb iso-

topic analyses were conducted using a 193 nm ArF excimer laser ablation system coupled with an Agilent 7500a ICP-MS (Agilent Technologies Inc., Santa Clara, CA, USA). Helium (He) served as the carrier gas for the ablated aerosol. The laser was operated with a beam diameter of 32 μm and a pulse width of 15 ns. Concentrations of U, Th, and Pb were calibrated using ^{29}Si as the internal standard, with reference values derived from NIST 610 glass. To ensure instrumental consistency, external standard calibration (using zircon reference material 91500) was performed after every 6 sample ablation spots, while NIST 610, 91500, and GJ-1 standards were analyzed after every 12 sample spots [19]. Data processing included the following: calculation of isotopic ratios and elemental concentrations using the GLITTER 4.0 software; age calculations and plotting of Concordia diagrams via Isoplot 3.0 [17,20]; and Pb correction using ComPbCorr#3_17. The in situ analysis of Lu-Hf isotopes in zircon was conducted based on the CL images of zircon. In situ isotopic measurements were performed using a Nu Plasma HR MC-ICP-MS (Nu Instruments) interfaced excimer laser ablation system (193 nm) under He carrier gas flow. The measurements were performed on the same points or domains of the previously dated zircons, which were analyzed using U-Pb isotopic methods. The analysis was carried out on the same points or domains of the previously dated zircons [21].

In calculating $\varepsilon_{Hf}(t)$ and T_{DM2}, the values for modern chondrites are cited from [22]. For the depleted mantle, the specific values can be found in another research study [23]. The decay constant for ^{176}Lu (λ) is taken as 1.867×10^{-11} a [24]. T_{DM2} is calculated using the upper crust values of $^{176}Lu/^{177}Hf = 0.0093$, with an $f_{Lu/Hf}$ of -0.72 [25]. In contrast, for the depleted mantle, an $f_{Lu/Hf}$ of 0.16 is used [23]. The formulas for calculating $\varepsilon_{Hf}(t)$, T_{DM2}, and $f_{Lu/Hf}$ are based on another study [26], with the operating conditions described by the authors of [27]. The results are listed in Tables S3 and S4 in the Supplementary Materials.

4. Results

4.1. Heavy Mineral Characteristics

Due to their relatively low abundance in sedimentary rocks and their minimal alteration from weathering and transport, heavy minerals are more effective in preserving information about parent rocks. Sedimentary heavy minerals from the same source area typically exhibit similar heavy mineral assemblages and comparable heavy mineral contents [28]. At the same time, the heavy mineral "fingerprint" of sediments under similar hydrodynamic conditions can reflect the characteristics of the source area's parent rocks [29]. Commonly used stable heavy mineral ratios include the ZTR, ATi, and GZi indexes. Therefore, heavy mineral assemblages, heavy mineral contents, and heavy mineral characteristic indices are among the methods used for provenance analysis.

Four of the five samples had high ZTR indices from 33.78 to 85.67 (average 61.64), and the ZTR index for sample LN-12 was 0.52. As the distance from the source rock area increases, the content of stable heavy minerals rises and maturity increases, resulting in a higher ZTR value [30,31]. The ATi and GZi indices for sample 16HC-01 are 0.16 and 0.07, respectively. For the remaining samples, both the ATi and GZi indices are 0.

For samples HC-01 and HC-12, heavy minerals are predominantly zircon (64.11% and 56.59%, respectively; Figure 2), followed by anatase (24.65% and 31.01%). For sample LN-03, heavy minerals are primarily goethite (34.01%), with zircon (30.66%) and anatase (27.15%) also present. In sample LN-12, goethite is the dominant heavy mineral (93.72%). In sample LN-20, zircon is the main heavy mineral (81.36%).

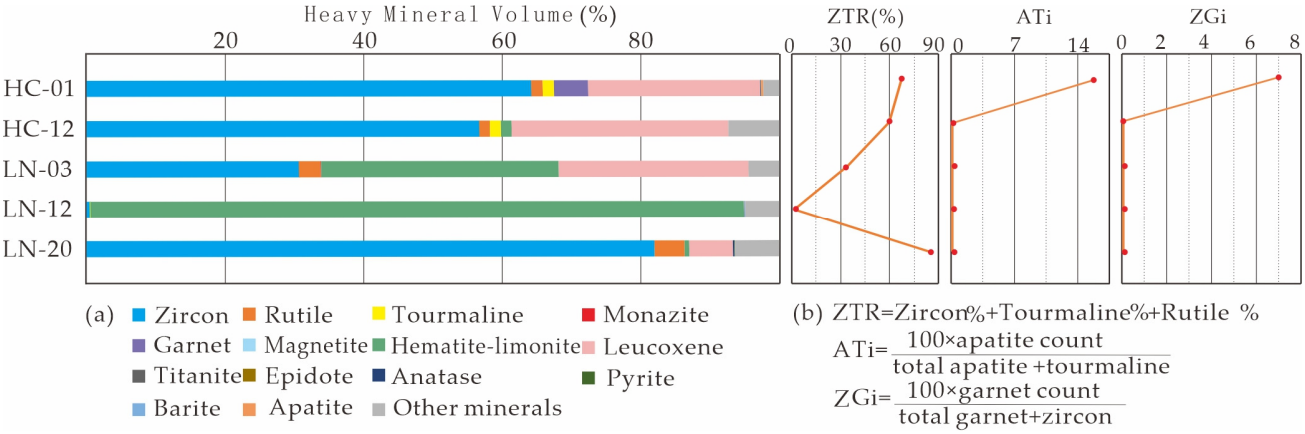


Figure 2. Heavy mineral assemblages (**a**) and heavy mineral indices (**b**) of the samples. Plotted with Excel 2016 and CorelDRAW Graphics Suite 2021 software, version 23.5.0.506.

4.2. Sedimentary Geochemistry Characteristics

4.2.1. Major Elements

For the samples of the Luonan region, the variation range of the major silicon element is small, with SiO_2 content ranging from 61.93% to 81.42% (average 70.03%), higher than the Post-Archean Australian shale (PAAS, SiO_2 = 59.52%; Taylor and McLennan, 1985 [32]) and the average upper crust value (UCC, SiO_2 = 66.62% [33]). In contrast, the Al_2O_3, Na_2O, K_2O, Na_2O/K_2O, and MgO contents of major elements are shown in Table 1.

Table 1. Major element contents of samples from the Shihezi Formation in Hancheng and Luonan.

Major Elements	Hancheng		Luonan		PAAS (wt%)
	Range (wt%)	Average (wt%)	Range (wt%)	Average (wt%)	
SiO_2	58.61–79.49	69.74	61.93–81.42	70.03	59.52
Al_2O_3	8.81–20.95	13.34	8.93–25.22	16.16	23.75
Na_2O	0.06–1.61	0.81	0.08–1.49	0.22	0.95
K_2O	0.28–2.01	1.00	0.43–9.28	3.69	3.44
MgO	0.54–1.34	0.82	0.04–1.26	0.54	1.81
TiO_2	0.30–0.97	0.64	0.41–0.84	0.63	1.03
CaO	0.24–2.83	0.65	0.02–0.37	0.17	0.57

For the samples of the Hancheng region, the variation range of the major element silicon is small, with SiO_2 content ranging from 58.61% to 79.49% (average 69.74%), higher than the Post-Archean Australian shale (PAAS, SiO_2 = 59.52% [32]) and the average upper crust value (UCC, SiO_2 = 66.62% [33]).

4.2.2. Trace Elements and Rare Earth Elements

Based on trace element data, the concentration ranges and average values for the sample of Luonan are shown in Table 2, with the original data available in Table S1. The trace element spider diagram exhibits a depletion of large-ion lithophile elements, with negative anomalies in Pb and Sr, characteristic of a mantle-derived signature (Figure 3).

Table 2. Trace element contents of samples from the Shihezi Formation in Hancheng and Luonan.

Element	Hancheng		Luonan		PAAS ($\times 10^{-6}$)
	Range ($\times 10^{-6}$)	Range ($\times 10^{-6}$)	Range ($\times 10^{-6}$)	Range ($\times 10^{-6}$)	
Sc	5.3–19.9	9.89	3.11–17.6	10.01	21
V	0.58–4.45	67.3	29.8–114	64.1	100
Cr	5.30–19.9	45.01	22.3–103	48.8	110
Ni	42.58–92.1	28.85	4.84–29.9	11.55	54
Ga	22.9–65.6	19.12	8.23–33.8	21.3	30
Rb	18.8–117	46.01	72.9–274	149	185
Sr	14.7–58.8	81.49	32.8–160	97	120
Zr	3.58–47.6	289	124–408	266	185
Nb	44.8–122	11.14	8.00–18.6	13.7	30
Cs	0.51–6.18	2.78	0.72–55.6	22.2	10
Ba	141–598	359	95.8–521	318	580
Hf	3.24–15.8	7.59	3.51–11.3	7.56	4.3
Pb	5.88–35.4	9.85	3.29–64.3	23.1	32
Th	5.46–13.1	9.99	6.90–19.8	11.67	19
U	1.19–3.33	2.35	1.51–5.33	3.09	3.3
La	15.6–144.4	47.41	18.44–291.29	73.42	50
Ce	24.99–260.9	89.79	38.90–510.22	130.95	104
Pr	2.47–29.28	9.91	4.53–57.87	15.67	13
Nd	8.7–119.1	48.12	15.92–229.59	60.08	43
Sm	1.67–22.17	8.73	3.21–41.64	10.79	8.2
Eu	0.36–4.51	1.65	0.59–7.01	1.90	1.7
Gd	1.56–20.38	7.85	2.71–39.42	9.69	6.7
Tb	0.24–2.76	1.12	0.39–5.34	1.34	1.2
Dy	1.49–14.36	6.26	2.22–28.48	7.44	6.2
Ho	0.29–2.76	1.2	0.45–5.19	1.40	1.4
Er	0.90–8.33	3.35	1.37–13.66	3.86	3.8
Yb	1.01–8.48	3.14	1.35–10.82	3.43	3.7
Y	7.64–49.15	31.32	12.01–136.90	36.13	38

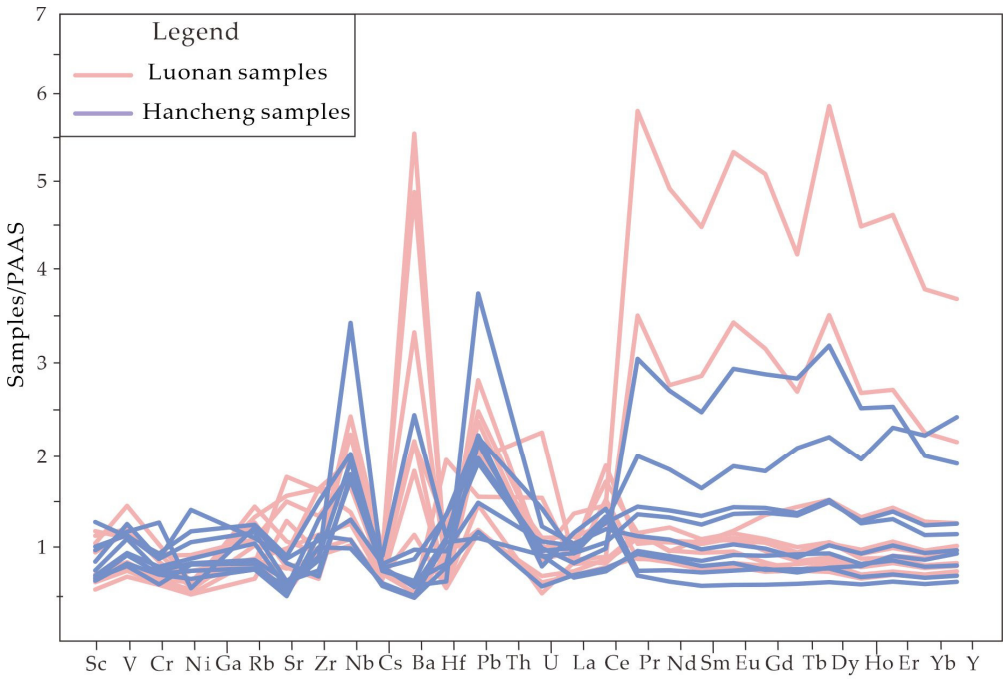


Figure 3. Trace element spider diagram (PAAS data from [32]; plotted with Origin 2021 software, version 9.8.0.200).

The samples of Luonan exhibit the following: La/Sc = 1.43 to 31.77 (average = 8.68), Th/Sc = 0.71 to 2.81 (average = 1.39), and Cr/Th = 2.54 to 6.46 (average = 4.09). These are much higher than the corresponding ratios in sediments derived from basic material source areas (La/Sc = 0.04 to 0.09; Th/Sc = 0.005 to 0.006; and Cr/Th = 1.10 to 1.15 [32]). These values consistently indicate that the sediments primarily originate from a more mature continental crust. Furthermore, the samples have a Th/U ratio ranging from 2.17 to 5.88 (average = 4.23). Because U is easily oxidized and leached during sedimentary and post-sedimentary processes, 70% of the samples from Luonan have Th/U ratios surpassing the canonical upper crustal reference (3.8). Therefore, the higher Th/U ratios likely reflect sediment recycling from earlier, pre-existing sediments through multiple depositional cycles. Low Th/Sc ratios may suggest a mafic provenance, whereas elevated Zr/Sc ratios likely reflect zircon enrichment, which is closely linked to sedimentary maturity. Pronounced LILE depletion in trace elements (Figure 3) is marked by pronounced negative anomalies in Rb, Sr, and Pb. These features potentially reflect either mantle-derived material influence in the source region or residual signatures from magmatic differentiation processes, such as those preserved in ancient cratonic basement lithologies. Significant zirconium enrichment (mean Zr = 26,655.04 $\times$ 10^{-6}) is observed, with elevated Zr/Sc ratios indicating pronounced zircon concentration. This enrichment correlates with sedimentary maturity and multi-cycle recycling processes, likely attributed to protracted sedimentary reworking or the inputs of ancient detrital zircons.

The concentration ranges and mean values of the samples from the Hancheng area are summarized in Table 2, with the original data available in Table S2.

The samples from Hancheng exhibit the following: La/Sc = 1.44 to 21.9 (average = 5.74); Th/Sc = 0.55 to 2.23 (average = 1.13); and Cr/Th = 2.82 to 5.85 (average = 4.59). These are much higher than the corresponding ratios in sediments derived from basic material source areas (La/Sc = 0.04 to 0.09; Th/Sc = 0.005 to 0.006; and Cr/Th = 1.10 to 1.15 [32]).

The analytical results of rare earth elements (REE) showed that the total amount of REE in the Luonan samples ranged from 106.45 $\times$ 10^{-6} to 1380.79 $\times$ 10^{-6}. In contrast, LREE/HREE = 2.57–5.99 (average 4.58), with LREE being enriched and HREE being in a deficit. Eu and Lu exhibit shallow values compared to the others. From the rare earth element distribution curves (Figure 4), a significant negative anomaly can be observed (Figure 4; δ_{Eu} = 0.52–0.70, average 0.59). Pronounced LREE/HREE fractionation is evident, with $(La/Yb)_N$ ratios spanning 5.12–22.28. Samples exhibit a rare earth element distribution pattern with a right-leaning negative europium anomaly similar to that of the continental crust.

The analytical results of rare earth elements (REEs) showed that the total amount of REE in the Hancheng samples ranged from 67.33 $\times$ 10^{-6} to 683.24 $\times$ 10^{-6} (average 239.43 $\times$ 10^{-6}), and LREE/HREE was =2.64–5.68, (an average of 4.49), with LREE being enriched and HREE being in a deficit. Eu and Lu exhibit low values compared to the others. From the rare earth element distribution curves (Figure 4), we can observe a significant negative anomaly (Figure 4; δ_{Eu} = 0.56–0.73, average 0.65). LREE/HREE fractionation is evident, with $(La/Yb)_N$ ratios spanning 7.31–17.92. The samples exhibit a rare earth element distribution pattern with a right-leaning negative europium anomaly.

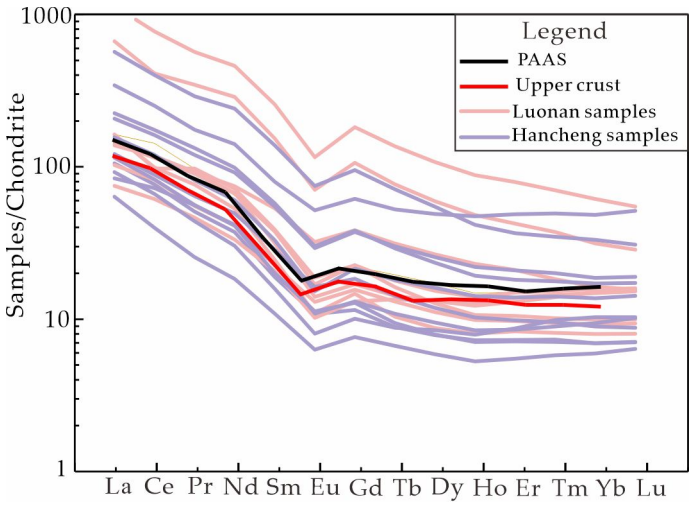


Figure 4. Rare earth elements' standardized partition curves (standardized data from [34]; plotted with Origin 2021 software, version 9.8.0.200 and CorelDRAW Graphics Suite 2021 software, version 23.5.0.506).

4.2.3. Provenance Area Weathering Conditions and Structural Background Discrimination

The chemical weathering index (CIA) of fine clastic rocks can be used to assess the intensity of chemical weathering and tectonic activity quantitatively [35]. A higher CIA value indicates that the rocks in the source area experienced more significant chemical weathering. Conversely, when the CIA value approaches 50, it suggests that the rocks in the provenance area have experienced little chemical weathering. The calculation formula for CIA is provided by the authors of [27].

The correction method for CaO^* is based on the authors of [36], and the corrections for K_2O are in accordance with the authors of [37]. The calculated CIA from the Luonan samples ranges from 65.70 to 92.75 (averaging 75.41). The calculated CIA from the Hancheng samples ranges from 63.31 to 90.03 (average 79.30), indicating that the source area has experienced significant chemical weathering. This suggests that the source area is in a tectonically stable environment with ongoing weathering processes. We need to consider excluding samples with strong weathering, and the CIA values should only be used as a reference.

According to the $K_2O/(Na_2O\text{-}SiO_2)$ (Figure 5) tectonic setting discrimination diagram [38], almost all Luonan samples fall within the passive continental margin field, indicating a relatively stable source region. Passive margin tectonic settings are inferred for five Hancheng samples and six samples from Hancheng, falling within the active continental margin field.

Roser et al. (1988) established source rock discrimination diagrams based on the major element compositions [39], which are used to identify the types of source rocks. The results indicate that the provenance of the Shihezi Fm of the Luonan mainly derives from felsic igneous source areas and quartzose recycled source areas, with mafic source areas and intermediate igneous sources being secondary (Figure 6). The Hancheng samples from the southern Ordos Basin are derived from the magnesium-iron pyroxene and quartz cyclotron source areas. This suggests that the source rocks are primarily from stable cratonic material, with a minor contribution from more active orogenic belt materials. The tectonic background of Luonan is not entirely the same as that of the source area in the southern Ordos Basin. Given the many factors influencing the major element compositions of sandstones and mudstones, the plotted results from the two types of discrimination diagrams may differ, and this result should be interpreted with caution.

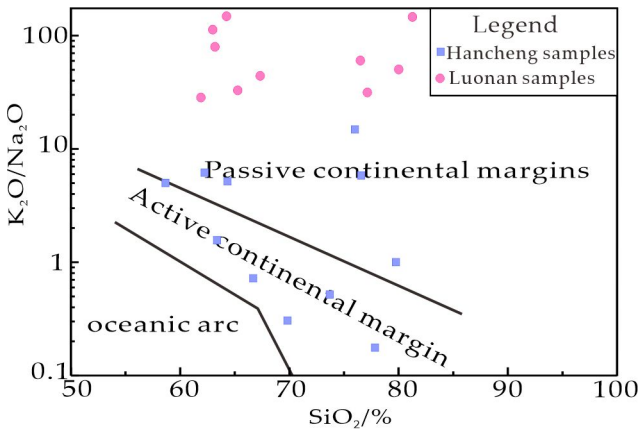
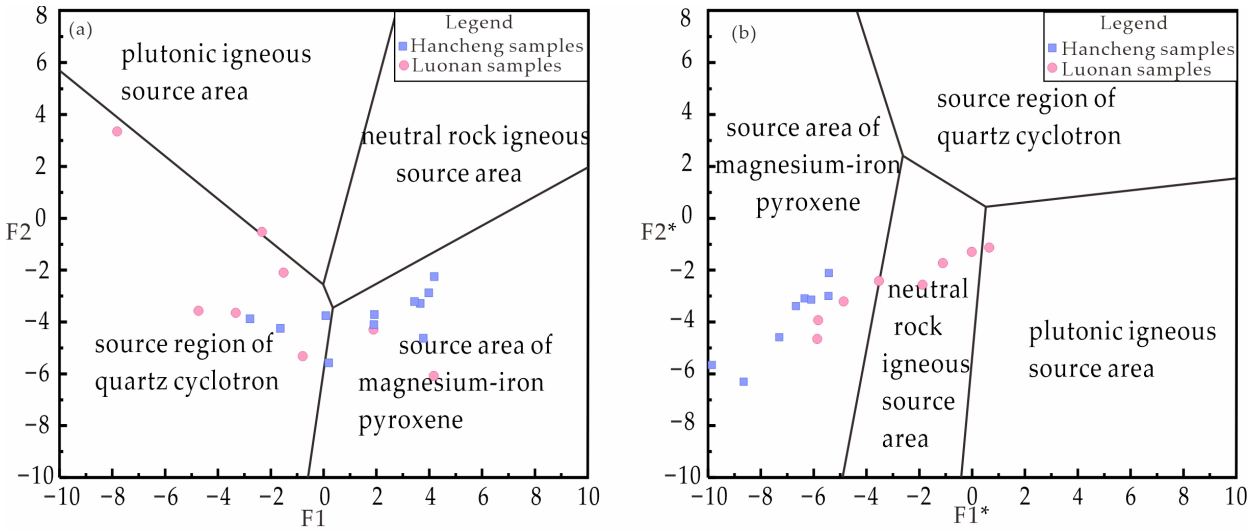


Figure 5. Major element-based tectonic setting discrimination diagram for the Shihezi Fm (the base map is modified from [38]; plotted with Origin 2021 software, version 9.8.0.200 and CorelDRAW Graphics Suite 2021 software, version 23.5.0.506.



$F1=-1.773TiO_2+0.607Al_2O_3+0.76Fe_2O_3(T)-1.5MgO+0.616CaO+0.509Na_2O-1.224K_2O-9.09$

$F2=0.445TiO_2+0.07Al_2O_3-0.25Fe_2O_3-1.142MgO+0.438CaO+1.475Na_2O+1.426K_2O-6.861$

$F1^*=30.638TiO_2/Al_2O_3-12.541Fe_2O_3(T)/Al_2O_3+7.329MgO/Al_2O_3+12.031Na_2O/Al_2O_3+35.402K_2O/Al_2O_3-6.382$

$F2^*=56.500TiO_2/Al_2O_3-10.879Fe_2O_3(T)/Al_2O_3+30.875MgO/Al_2O_3-5.404Na_2O/Al_2O_3+11.112K_2O/Al_2O_3-3.890$

Figure 6. Provenance discrimination plot for the major element compositions of Luonan and Hancheng samples. (**a**) F1-F2 discriminant diagram for rock provenance classification, (**b**) F1*-F2* discriminant diagram for rock provenance classification (the base maps are modified from [39]; plotted with Origin 2021 software, version 9.8.0.200 and CorelDRAW Graphics Suite 2021 software, version 23.5.0.506).

Provenance tectonic settings are identified through the La-Th-Sc and Th-Sc-Zr/10 diagrams [40] (Figure 7). The samples from the Luonan area predominantly fall within the continental island arc region, with a small portion located in the active and passive continental margin regions. In total, 80% of the Hancheng samples exhibited continental arc affinities, and one sample fell within the passive continental margin. Considering that the sediments from passive continental margins can also contain significant information from continental magmatic arcs, the discrimination results can be compared with the K_2O/Na_2O-SiO_2 diagram (Figure 5). This comparison indicates that the clastic material in the Luonan area mainly originates from a tectonic setting of continental magmatic arcs and passive continental margins.

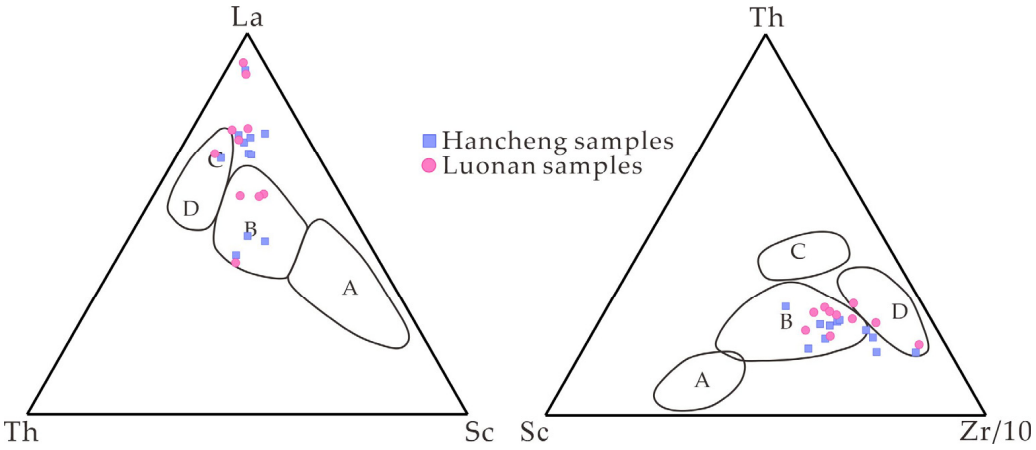


Figure 7. Tectonic setting discrimination diagrams (La-Th-Sc and Th-Sc-Zr/10) for the provenance analysis of the Shihezi Fm (A—oceanic arc; B—continental arc; C—active continental margin; D—passive continental margin. The base maps are modified from [40]; plotted with Origin 2021 software, version 9.8.0.200 and CorelDRAW Graphics Suite 2021 software, version 23.5.0.506).

4.3. Zircon U-Pb Geochronology

Cathodoluminescence (CL) imaging reveals that Hancheng zircons exhibit prismatic morphologies with dominant oscillatory zoning (Figure 8a) and magmatic Th/U > 0.4, which are diagnostic of magmatic zircon crystallization processes. It can be observed that the zircon grains in the Luonan sample are predominantly round to rounded (Figure 8b number: 123), with a smaller proportion being angular to sub-angular (Figure 8b number: 111). Most of the zircon grains show significant rounding. This likely indicates that the zircon grains experienced prolonged physical abrasion during transport and deposition. The internal structure features are predominantly oscillatory zoning (Figure 8b,c), with Th/U > 0.4, indicating typical magmatic origin zircons. Our samples have 376 zircon grains selected for analysis in this test, with laser spots chosen at clean and clear locations to exclude the influence of cracks and inclusions on the samples.

In total, the harmony degree of 280 zircon grains with 90%–110% concordance is deemed acceptable. The Concordia plot shows that the U-Pb age data fall on or near the Concordia line (Figure 9), indicating good sample concordance and high result reliability.

For sample HC-01, the U-Pb ages of 102 zircons (n = 102) were geochronologically analyzed (one spot per grain), with 53 of these analyses extended to Lu-Hf isotopic characterization to constrain source terrane evolution. Among these, 86 zircon grains yielded concordant ages. These zircons reveal three prominent age peaks as follows: The first group spans approximately 270 Ma to 418 Ma (peak: 315 Ma) (Figure 10a); the second group spans approximately 1710 Ma to 2072 Ma and exhibits a major peak at 1886 Ma; and the third group spans approximately 2233 Ma to 2549 Ma and exhibits a major peak at 2485 Ma. The first group's zircons display heterogeneous Th/U ratios (0.05–1.50), with one spot falling below 0.1 and one zircon ranging from 0.1 to 0.4. The second group has Th/U ratios at 0.14–1.93, with six spots ranging from 0.1 to 0.4. The third group shows Th/U values from 0.12 to 1.61, with one spot ranging from 0.1 to 0.4. Additionally, sample HC-01 had a zircon grain with a Th/U ratio of < 0.1. This zircon grain had a grain age of 270 Ma.

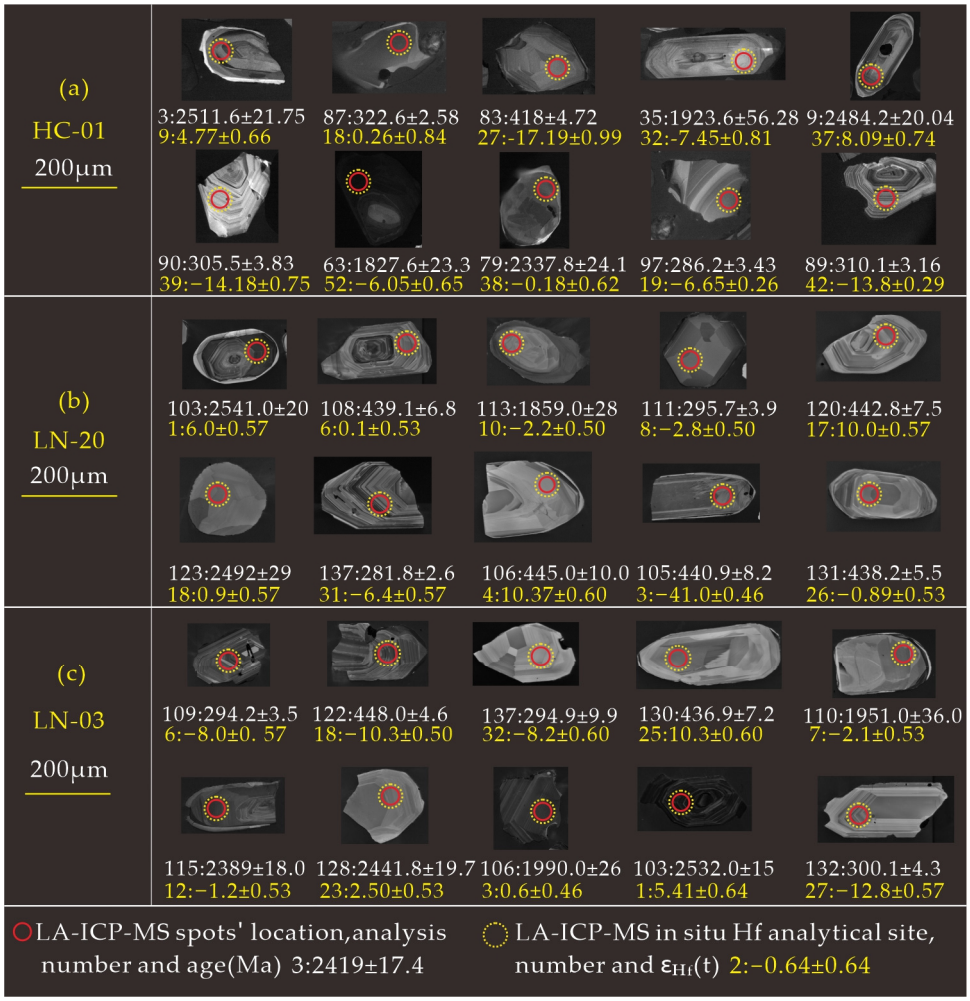


Figure 8. Typical detrital zircon CL images of the Shihezi Fm in Hancheng (**a**) and Luonan (**b**,**c**) area. Plotted with CorelDRAW Graphics Suite 2021 software, version 23.5.0.506.

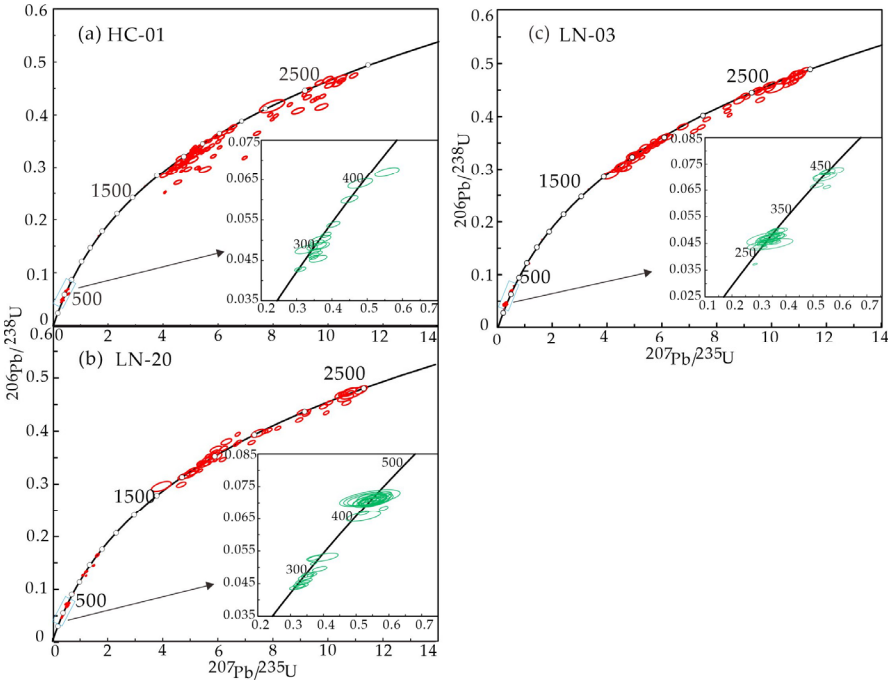


Figure 9. Results of detrital zircon U-Pb Concordia diagrams. Plotted with Isoplot software, version 4.15.

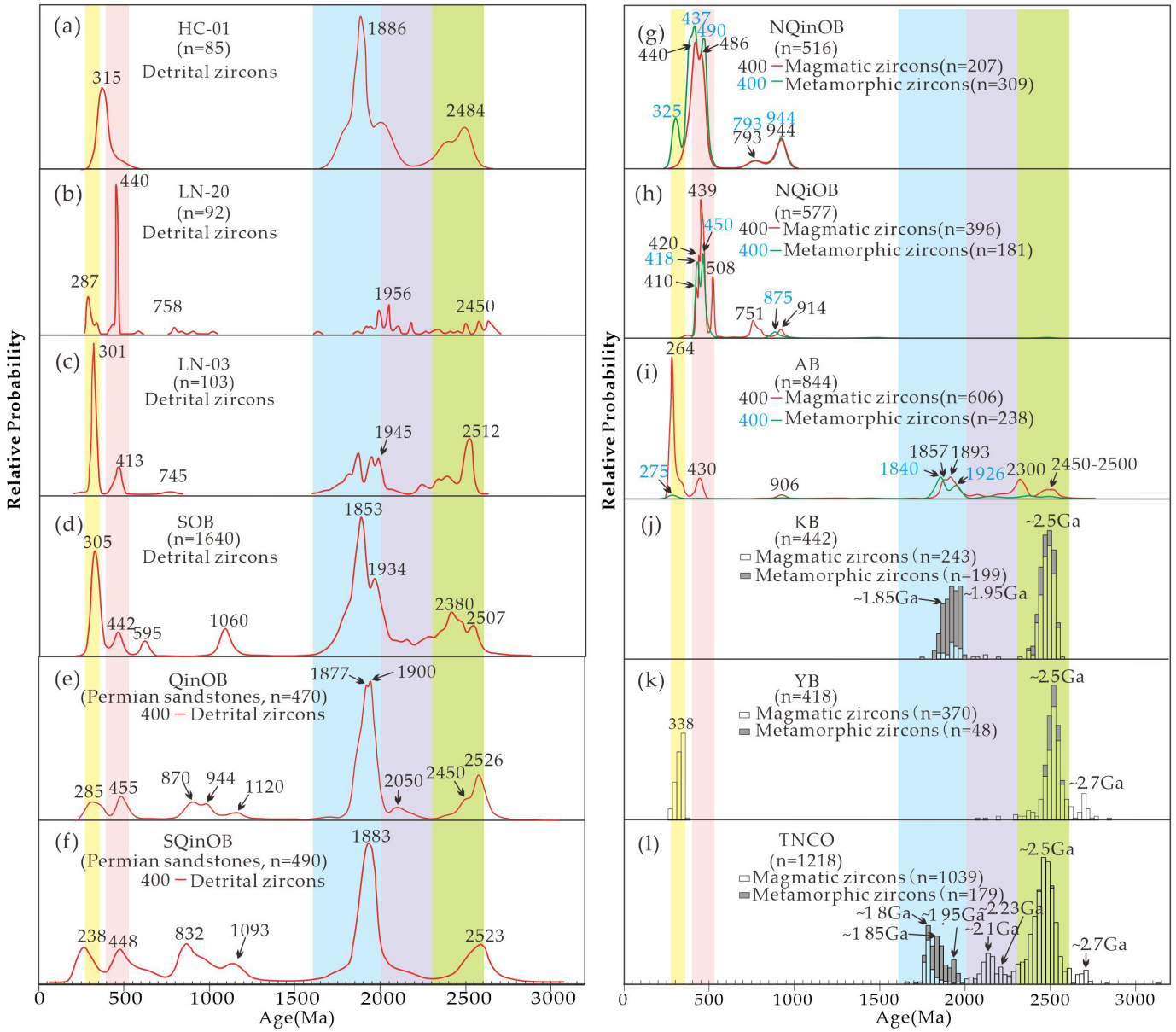


Figure 10. Results of detrital zircon U-Pb age histograms. (**a**) Age spectrum of Sample HC-01 from the study area, (**b**) Age spectrum of Sample LN-20 from the study area, (**c**) Age spectrum of Sample LN-03 from the study area, (**d**) Age spectrum of SOB, (**e**) Age spectrum of QinOB, (**f**) Age spectrum of SQinOB, (**g**) Age spectrum of NQinOB, (**h**) Age spectrum of NQiOB, (**i**) Age spectrum of AB, (**j**) Age spectrum of KB, (**k**) Age spectrum of YB, (**l**) Age spectrum of TNCO. Only the ages with lower than 10% discordance were used. The yellow, pink, blue, gray, and green bars show the age groups of 350–268 Ma, 520–386 Ma, 2000–1600 Ma, 2300–2000 Ma, and 2600–2300 Ma, respectively. (**a**–**c**) show data from this study. The detrital zircon ages of the SQinOB are from the authors of [41,42]; the magmatic zircon and metamorphic zircon ages of the NQinOB, Trans–North China Orogenic Belt (TNCO), NQiOB, Alxa Block (AB), Khondalite Belt (KB), and Yinshan Block (YB) are from the authors of [43] and the references therein; the detrital zircon ages of the QinOB and southern Ordos Basin (SOB) are from the authors of [43] and the references therein; and the LN-03, LN-20, and HC-01 data are from this study. The relative probability curves were drawn with the DensityPlotter program (version 8.5), using the kernel density estimation model (KED). The width of one column in (**j**–**l**) is 25 Ma. Plotter with Density Plotter software, version 8.5 and CorelDRAW Graphics Suite 2021 software, version 23.5.0.506.

For sample LN-20, the U-Pb ages of 137 zircons (n = 137) were geochronologically analyzed (one spot per grain), with 31 of these analyses extended to Lu-Hf isotopic characterization to constrain source terrane evolution. Among these, 93 zircon grains yielded concordant ages. Ninety-two zircon U-Pb ages were acquired from the LN-20 sandstone samples. These zircons reveal the following three prominent age peaks: the first group spans approximately 277 Ma to 451 Ma, with peaks at 440 Ma and 287 Ma (Figure 10b); the second group spans approximately 560 Ma to 979 Ma and reveals a major peak at 758 Ma; and the third group spans approximately 1784 Ma to 2560 Ma and exhibits peaks at 1956 Ma and 2450 Ma. The zircons in the first group has a Th/U ratio from 0.01 to 1.1, and three spots fall below 0.1, with seven zircons ranging from 0.1 to 0.4. The second group has a Th/U ratio from 0.37 to 0.73 and two spots falling below 0.4. The third group has Th/U ratios ranging from 0.04 to 2.35, with one spot falling below 0.1 and two zircons ranging between 0.1 and 0.4. Additionally, sample LN-20 contains four zircons with Th/U ratios of <0.1. These zircon grains yield ages of 287 Ma, 300 Ma, 322 Ma, and 2086 Ma.

For sample LN-03, the U-Pb ages of 137 zircons (n = 137) were geochronologically analyzed (one spot per grain), with 32 of these analyses extended to Lu-Hf isotopic characterization to constrain source terrane evolution. Among these, 103 zircon grains yielded concordant ages. A total of 103 zircon U-Pb ages were acquired from the LN-03 sandstone samples. These zircons reveal the following three prominent age peaks: the first group spans from approximately 235 Ma to 450 Ma and features peaks around 300 Ma and 437 Ma (Figure 10c); the second group covers an age range from about 1663 Ma to 2079 Ma and exhibits peaks at 1945 Ma; and the third group spans from approximately 2237 Ma to 2555 Ma, exhibiting a peak at approximately 2517 Ma. The zircons in the first group have a Th/U ratio from 0.33 to 1.22, with four falling below 0.4, indicating a predominantly magmatic origin for these zircons. In the second group, Th/U values from 0.06 to 2.58 were observed, including two values below 0.1 and three zircons between 0.1 and 0.4. The third group has Th/U values from 0.22 to 1.45, with two spots < 0.4, suggesting mid-stage metamorphic overprinting with varying intensities in a subset of zircons. Additionally, sample LN-03 contains two zircons with Th/U < 0.1. These zircons provide ages of 1777 Ma and 1937 Ma, indicating that the zircon grains underwent varying degrees of metamorphic alteration during earlier and later periods.

4.4. In Situ Zircon Hf Isotopic Analyses

Detrital zircons from sample HC-01 (n = 53) yield $\varepsilon_{Hf}(t)$ values from −17.19 to 8.09 (mean: −3.29), reflecting a mixture of ancient crustal reworking and juvenile magmatic contributions, with T_{DM2} between 1311 Ma and 3136 Ma (average 2529 Ma). Among these, 17 grains show positive $\varepsilon_{Hf}(t)$ values (0.02 to 8.09) accompanied by T_{DM2} ages of 1311–2907 Ma, while 36 grains display negative $\varepsilon_{Hf}(t)$ values (−17.19 to −0.10) and T_{DM2} ages spanning 1378–3136 Ma. Within the 2600–2300 Ma age cohort (15 grains), two zircon grains record negative $\varepsilon_{Hf}(t)$ values (−0.18 and −1.39) with Paleoarchean T_{DM2} ages (2880–2955 Ma), while the remaining 13 grains exhibit positive $\varepsilon_{Hf}(t)$ values from 0.02 to 8.09 and T_{DM2} ages of 2488–2955 Ma. The 2300–2000 Ma population (6 grains) contains five zircons with negative $\varepsilon_{Hf}(t)$ values (−0.18 to −3.83) and T_{DM2} values of 2656–2867 Ma, contrasted by a single zircon showing $\varepsilon_{Hf}(t)$ = 2.33 with T_{DM2} = 2688 Ma. For the 2000–1600 Ma interval (17 grains), 15 zircons display negative $\varepsilon_{Hf}(t)$ values (−0.10 to −10.44) and T_{DM2} values of 2509–3136 Ma, while three grains exhibit positive $\varepsilon_{Hf}(t)$ values (2.88 to 3.93) corresponding to younger T_{DM2} ages of 2369–2327 Ma. The 550–350 Ma group (three grains) is exclusively characterized by negative $\varepsilon_{Hf}(t)$ values (−17.19, −10.26, and −10.41), with T_{DM2} values of 2479 Ma, 2024 Ma, and 2033 Ma. Finally, within the 350–260 Ma population (12 grains), 11 zircons show negative $\varepsilon_{Hf}(t)$ values (−14.64 to −0.61) and T_{DM2} values

of 1378–2222 Ma, contrasted by a single grain with an $\varepsilon_{Hf}(t)$ value of 0.26 and T_{DM2} of 1311 Ma.

Hf isotopic compositions were characterized in 63 detrital zircons (Luonan sample) to constrain their petrogenetic evolution, with their age-specific distributions and isotopic signatures categorized as follows: 2750–2300 Ma cohort (n = 8) $\varepsilon_{Hf}(t)$ values from −2.7 to 6.0 (mean: 2.4), with corresponding T_{DM2} model ages ranging from 2591 to 2941 Ma (mean: 2823 Ma; Figure 11). Three grains exhibit negative $\varepsilon_{Hf}(t)$ (−2.7 to −0.3; T_{DM2}: 2984–3037 Ma). Five grains display positive $\varepsilon_{Hf}(t)$ (0.9 to 6.0; T_{DM2}: 2591–2941 Ma). In the 2100–1760 Ma cohort (n = 18), negative $\varepsilon_{Hf}(t)$ values (−9.5 to −1.0; T_{DM2}: 2509–3127 Ma) dominated in 16 grains. Two exceptions show positive $\varepsilon_{Hf}(t)$ (0.6, 3.1) values with younger T_{DM2} ages (2406–2569 Ma). In the 1200–770 Ma cohort (n = 1), a single grain yields $\varepsilon_{Hf}(t)$ = −1.6 and T_{DM2} = 1928 Ma. In the 512–256 Ma cohort (n = 32), broad $\varepsilon_{Hf}(t)$ variability (−41.0 to 13.0; mean: −4.07) and T_{DM2} spreads (596–3940 Ma; mean: 1623 Ma) were observed. In 19 grains, negative $\varepsilon_{Hf}(t)$ values were prevalent (−41.0 to −0.9; T_{DM2}: 1473–3940 Ma). In 13 grains, positive $\varepsilon_{Hf}(t)$ values were prevalent (0.1 to 13.0; T_{DM2}: 596–1410 Ma).

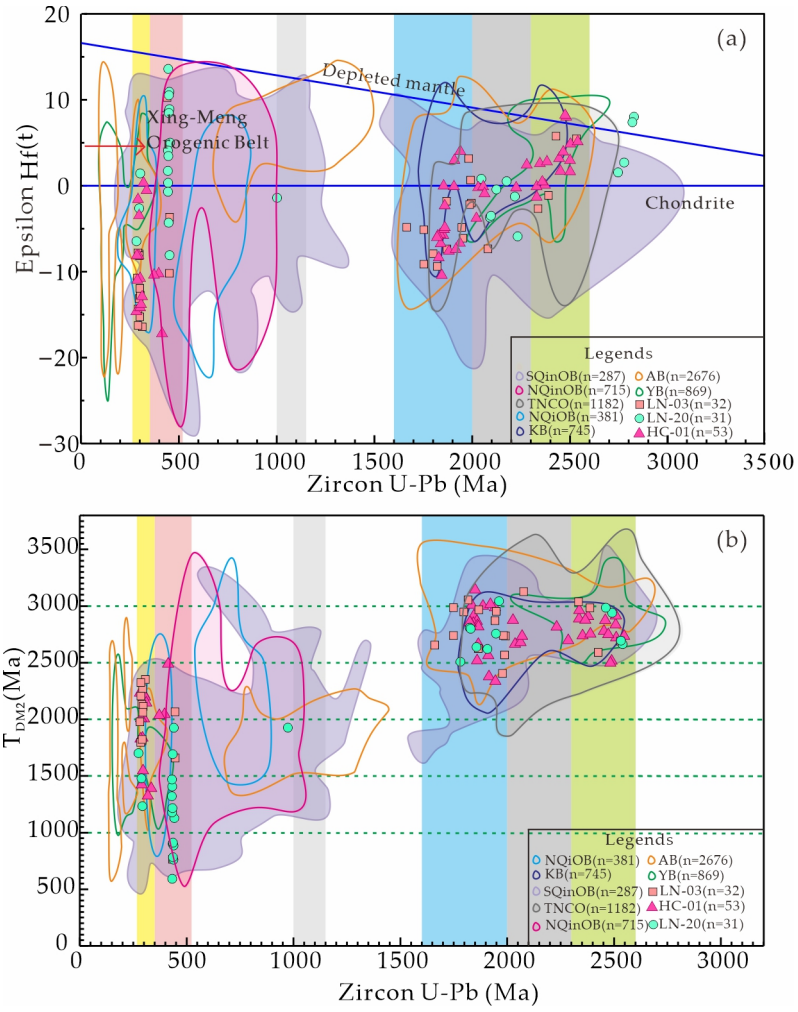


Figure 11. $\varepsilon_{Hf}(t)$ values vs. U-Pb ages (**a**) and T_{DM2} vs. U-Pb ages (**b**). The yellow, orange, blue, gray, and green bars show the age groups of 350–268 Ma, 520–386 Ma, 2000–1600 Ma, 2300–2000 Ma, and 2600–2300 Ma, respectively. The SQinOB data are from the authors of [41,42]; the NQinOB, Trans–North China Orogenic Belt (TNCO), NQiOB, Khondalite Belt (KB), Yinshan Block (YB), and Alxa Block (AB) data are from the authors of [43] and the references therein; the LN-03, LN-20, and HC-01 data are from this study. Data on depleted mantle from [23]. Plotted with Origin 2021 software, version 9.8.0.200 and CorelDRAW Graphics Suite 2021 software, version 23.5.0.506.

5. Discussion

5.1. Provenance of Heavy Minerals

The Luonan area is mineralogically characterized by zircon, leucoxene, and hematite-limonite assemblages. The ZTR index of the samples exhibits a clear trend as follows: the highest ZTR in the LN-20 sample implies a distal position of LN-20 relative to the provenance compared to other samples. This suggests that the provenance material is relatively mature and stable, likely originating from a stable source area farther from the sedimentary basin. The high ZTR value indicates that the sample's source area has undergone significant weathering, and the material likely comes from a distant source, possibly having been transported from a more remote sedimentary source. The lowest ZTR is LN-03, which is only 0.52. This means that the source area of the LN-03 sample is relatively close to the sedimentary basin, indicating a more active tectonic setting or a younger source area. The provenance material is relatively young or has not undergone extensive weathering. Hancheng is mainly dominated by zircon, leucoxene, rutile, and tourmaline, and it also contains garnet and hematite-limonite. The heavy mineral composition, assemblage types, and spatial distribution patterns of the Shihezi Fm in Luonan (North China Block) exhibit significant similarities to those of the Shihezi Fm in Hancheng.

The Luonan heavy mineral assemblage is dominated by zircon + hematite-limonite + leucoxene, whereas the Hancheng assemblage primarily comprises zircon + leucoxene + rutile + tourmaline, with sporadic occurrences of garnet—a feature absent in Luonan but replaced by hematite-limonite. This distinct mineralogical divergence indicates shared provenance sources between the two regions, alongside contributions from distinct source terranes.

The quantitative analysis of heavy mineral indices reveals that the ZTR index (zircon-tourmaline-rutile index) in Hancheng exceeds that of Luonan, suggesting a progressive diminution in stable heavy mineral content and sediment maturity from Hancheng to Luonan. Furthermore, the higher ATi index (apatite-tourmaline index) and GZi index (garnet-zircon index) values in the Hancheng samples imply dominant sediment derivation from intermediate-acidic igneous rocks, with limited supply from low-grade to medium-grade metamorphic source rocks. These findings collectively demonstrate systematic provenance differentiation between the Luonan and Hancheng depositional systems.

5.2. Provenance of Geochemical Analysis

Comparative provenance analysis based on major element geochemistry shows the following: Integrated major element characteristics from the Luonan and Hancheng areas reveal distinct source-to-sink system evolutionary pathways. Luonan provenance is dominated by felsic rocks typical of cratonic or stable continental margin settings, as evidenced by elevated SiO_2/Al_2O_3 and K_2O/Na_2O ratios, and strong chemical weathering signatures (CIA > 80) are likely derived from Proterozoic basement rocks exposed along the southern margin of the TNCO. Hancheng provenance exhibits hybrid source characteristics with predominant felsic components (SiO_2 > 65%), and subordinate inputs from intermediate-acidic volcanic rocks or metamorphic lithologies reflect localized Mesozoic tectonic-magmatic overprinting, possibly associated with subduction-related arc magmatism and intracontinental reactivation events. The trace element characteristics of the Luonan and Hancheng areas reveal distinct geological signatures, as follows: Luonan exhibits high La/Sc and Th/Sc ratios, consistent with passive continental margins or stable intracratonic sedimentary basins. In contrast, Hancheng samples exhibit low Th/Sc and moderate La/Sc ratios, indicative of an active continental margin or island arc environment, with source rocks likely derived from Late Paleozoic metamorphic basic rocks in the Qinling Orogenic Belt.

The Luonan area exhibits LREE enrichment and HREE depletion, indicative of source rocks dominated by felsic rocks with high differentiation degrees or multi-cycled sedimen-

tary materials. The observed Eu negative anomalies in the Luonan samples align with upper continental crust characteristics, reflecting the recycling of ancient sedimentary rocks in the source region. The strong LREE fractionation further supports the interpretation of mature continental crustal sources. The overall REE distribution patterns show right-leaning trends with pronounced Eu anomalies, consistent with typical continental crustal REE signatures. In contrast, Hancheng samples display lower total REE concentrations compared to Luonan, with comparable LREE enrichment but distinct geochemical features as follows: The HC-11 sample shows a LREE/HREE ratio of <4 and weaker Eu anomalies (less pronounced than Luonan). The right-leaning REE patterns with Eu anomalies resemble continental crustal signatures. However, combined with low Th/Sc ratios (0.11) and localized Cr anomalies, these features suggest possible mafic source contributions. The geochemical signatures are consistent with an active continental margin or back-arc basin setting. The Late Paleozoic–Mesozoic tectonic reactivation likely triggered diverse source inputs, involving both cratonic basement materials and subduction-related magmatic rocks.

Luonan provenance reflects felsic basement rocks from the southern margin of the TNCO, subjected to intense chemical weathering and multi-cycle sedimentary recycling, with a tectonic setting dominated by a stable Craton or passive margin. The provenance contrast between Luonan and Hancheng highlights a transition from stable cratonic conditions (Luonan) to an active tectonic zone (Hancheng) along the southern TNCO, potentially linked to Mesozoic tectonic overprinting associated with the Qinling orogenic belt.

5.3. Provenance of Detrital Zircons

The zircon age spectra reflect the recycling of stable continental crust basement material and materials associated with more active continental orogenic belts, which is well recorded and reflected in the detrital zircon characteristics of the Luonan sandstones. Overall, the detrital zircon age of the Luonan Shihezi Fm are characterized by two main zircon age groups as follows: the Paleoproterozoic (2600–1700 Ma), with a small amount of Neoarchean (Figure 10b,c), and the Paleozoic (550–270 Ma), along with a small number of zircons with Neoproterozoic ages (750–550 Ma). The proportion of Paleoproterozoic zircons is higher than that of the Paleozoic zircons, indicating that the primary material source is from ancient continental crust, with a certain amount of relatively younger material from orogenic belts.

The Shihezi Fm of Hancheng sample HC-01 exhibits the following three age groups: 418–270 Ma, 1819–1710 Ma, and 2511–1836 Ma (Figure 10a). Luonan sample LN-20 exhibits the following five age groups: 277–416 Ma, 426–451 Ma, 560–979 Ma, 1563–1784 Ma, and 1827–2560 Ma (Figure 10b). Luonan sample LN-03 exhibits six age groups as follows: 235 Ma, 273.9–416 Ma, 436–449 Ma, 744 Ma, 1663–1751 Ma, and 1802–2537 Ma (Figure 10c).

Sedimentation postdates the youngest concordant zircon age, providing a temporal upper limit [44,45]. In this study, the youngest age obtained is 235 ± 1 Ma of sample LN-03 from the Shihezi Fm (Figure 10c). The zircon exhibits a concordance value of 108.1%, exceeding the ±10% threshold adopted in this study. While some researchers employ stricter concordance criteria (±5%), we exclude this 235 Ma zircon from geochronological interpretation due to its significant discordance, rendering it geologically nonindicative.

(1) Archaeozoic–Middle Archean zircons (2600–1600 Ma)

In Luonan samples, forty-five detrital zircons (23.07%, n = 195) yield 2600–2300 Ma, The majority of these zircons display characteristic magmatic oscillatory zoning. The Lu-Hf isotopic analysis of eight grain features is shown in Table 3, and zircons from the Luonan area, dated 2600–2300 Ma, display both positive and negative $\varepsilon_{Hf}(t)$ values, indicating the possible coexistence of ancient crustal reworking and the input of juvenile crustal materials during magma generation. This bimodal $\varepsilon_{Hf}(t)$ signature suggests a hybrid magmatic

source involving contributions from recycled ancient crustal components (negative $\varepsilon_{Hf}(t)$) and new mantle-derived melts (positive $\varepsilon_{Hf}(t)$).

Table 3. Summarized Hf isotopic composition and two-stage model age.

Ages (Ma)	Parameters	HC Samples	LN Samples
2600–2300	Negative $\varepsilon_{Hf}(t)$ value	−0.18 to −1.39	−2.7 to −0.3,
	T_{DM2} value	2880–2955 Ma	2984–3037 Ma
	Positive $\varepsilon_{Hf}(t)$ value	0.02 to 8.09	0.9 to 6.0
	T_{DM2} value	2488–2955 Ma	2591–2941 Ma
2300–2000	Negative $\varepsilon_{Hf}(t)$ value	−0.18 to −3.83	−7.4
	T_{DM2} value	2656–2867 Ma	3127 Ma
	Positive $\varepsilon_{Hf}(t)$ value	2.33	50
	T_{DM2} value	2688 Ma	409 Ma
2000–1600	Negative $\varepsilon_{Hf}(t)$ value	−0.1 to −10.44	−9.5 to −1.0
	T_{DM2} value	2509–3136 Ma	2509–3054 Ma
	Positive $\varepsilon_{Hf}(t)$ value	2.88 to 3.93	0.6 to 3.1
	T_{DM2} value	2369–2327 Ma	2568–2406 Ma
979–550	Negative $\varepsilon_{Hf}(t)$ value	/	−1.6
	T_{DM2} value	/	1928 Ma
	Positive $\varepsilon_{Hf}(t)$ value	/	/
	T_{DM2} value	/	/
550–350	Negative $\varepsilon_{Hf}(t)$ value	−17.19 to −10.26	−41 to −0.9
	T_{DM2} value	2480–2030 Ma	1473–3940 Ma
	Positive $\varepsilon_{Hf}(t)$ value	/	0.1–13.0
	T_{DM2} value	/	596–1410 Ma
350–260	Negative $\varepsilon_{Hf}(t)$ value	−14.64 to −0.61	−16.5 to −2.8
	T_{DM2} value	1378–2222 Ma	1482–2351 Ma
	Positive $\varepsilon_{Hf}(t)$ value	0.26	1.2
	T_{DM2} value	1311 Ma	1237 Ma

In the Hancheng sample, sixteen detrital zircons (18.6%, n = 86) yield 2600–2300 Ma within the 2600–2300 Ma age cohort (15 grains). The Lu-Hf isotopic analysis of eight grain features is shown in Table 3. The Luonan area shows a significantly higher proportion of zircons in the 2600–2300 Ma age range (22.28%) compared to Hancheng (8.29%). This disparity suggests distinct provenance differences as follows: Luonan's dominant contributions are likely derived from the ancient basement of the TNCO, as elevated Neoarchean–Paleoproterozoic zircon populations are characteristic of cratonic reworking. The Yinshan region is dominated by magmatic activity at ~2.7 Ga, whereas the Luonan–Hancheng area exhibits a more pronounced peak at ~2.5 Ga, suggesting a closer affinity to the internal basement of the TNCO. In the Luonan sample, sixteen detrital zircons (8.20%, n = 195) yield Paleoproterozoic U-Pb ages (2300–2000 Ma), with over 85% (n = 16) exhibiting magmatic oscillatory zoning. Two grains from the Shihezi Fm were further analyzed for Lu-Hf isotopes, yielding $\varepsilon_{Hf}(t)$ values spanning from −7.4 to 50 and a T_{DM2} between 409 Ma and 3127 Ma.

In the Hancheng sample, nine detrital zircons (10.46%, n = 86) yield Paleoproterozoic U-Pb ages (2300–2000 Ma). The majority of these grains preserve well-defined oscillatory zoning textures, which are diagnostic of primary magmatic crystallization processes. The Lu-Hf isotopic analysis of eight grain features is shown in Table 3. Even though the peak of the sample at this age is similar to the Khondalite Belt (KB, Figure 10j), zircons from the Khondalite Belt during the ~1.95 Ga metamorphic event predominantly exhibit positive $\varepsilon_{Hf}(t)$ values [21], whereas those of the same age cohort in the Luonan area are characterized

by predominantly negative $\varepsilon_{Hf}(t)$ values. This isotopic contrast suggests no significant provenance contribution from the Khondalite Belt to Luonan during this period.

In the Luonan sample, 55 detrital zircons (28.20%, n = 195) yield 2000–1600 Ma. The majority of these grains preserve well-defined oscillatory zoning textures, which are diagnostic of primary magmatic crystallization processes. A total of 20 zircons in the Shihezi Fm underwent Lu-Hf isotopic examination, and the Lu-Hf isotopic analysis of eight grain features is shown in Table 3. Zircons from the Luonan area within the 2000–1600 Ma age range exhibit predominantly negative $\varepsilon_{Hf}(t)$ values coupled with older T_{DM2} model ages, indicating dominant crustal reworking processes during this period. This geochemical signature implies the following: limited contribution from juvenile mantle-derived materials and the predominance of the recycling-reworking of pre-existing ancient crustal components; tectonic stability with minimal magmatic accretion events in the source region.

In the Hancheng sample, 44 detrital zircons (51.11%, n = 86) yield 2000–1600 Ma. For the 2000–1600 Ma interval (17 grains), the Lu-Hf isotopic analysis of eight grain features is shown in Table 3. Zircons from Hancheng within the 2000–1600 Ma age range are predominantly characterized by negative $\varepsilon_{Hf}(t)$ values, with minor occurrences of positive $\varepsilon_{Hf}(t)$ values. This bimodal distribution may suggest the localized incorporation of juvenile crustal materials alongside dominant crustal reworking processes. For the period from ~1.95 to ~1.80 Ga, TNCO experienced metamorphisms associated with the collision of the eastern and western blocks of the TNCO [13]. Even though the peak of the sample at this age is similar to the Khondalite Belt (Figure 10j), zircons from the Khondalite Belt predominantly exhibit positive $\varepsilon_{Hf}(t)$ values during the ~1.85 Ga post-collisional extension phase [21], whereas those from the Luonan and Hancheng areas within the same age interval are characterized by predominantly negative $\varepsilon_{Hf}(t)$ values (Figure 11a). This isotopic discrepancy provides evidence against a provenance linkage between the Khondalite Belt and the Luonan–Hancheng regions. Consequently, we propose that the detrital materials of this age range in Luonan and Hancheng were derived from the TNCO.

According to previous studies on the paleocurrent direction of Hancheng, the paleocurrent direction of Hancheng is dominated by W and NW [46], implying that the clastic material filling Hancheng during the depositional period of the Shihezi Fm was derived from the denudation source area of the main uplift material in the southeast. Integrated studies of paleocurrent directions and heavy mineral assemblages (Figure 2) in the southern Ordos Basin demonstrate that the Shihezi Fm sediments were not sourced from the northern basin margins [27,42]. Consequently, the Yinshan Block (YB) and Alxa Block (AB) are excluded as provenances for the Luonan and Hancheng regions.

(2) Neoproterozoic zircons (979–550 Ma)

In the Luonan sample, seven detrital zircon grains (3.58%, n = 195) fall within the 979–550 Ma age range. The petrographic analysis reveals that over 85% of this population (n = 7) preserves distinct magmatic oscillatory zoning, characteristic of primary crystallization processes. The Lu-Hf isotopic analysis of eight grain features is shown in Table 3. This signature may correlate with Neoproterozoic magmatic activity in the NQinOB, potentially reflecting Neoproterozoic magmatism in NQinOB.

(3) Paleozoic zircons (550–350 Ma)

In the Luonan sample, seven detrital zircon grains (15.89%, n = 195) fall within the 550–350 Ma age range. The majority of these grains preserve well-defined oscillatory zoning textures, diagnostic of primary magmatic crystallization processes. Eight zircon grains extracted from the Shihezi Fm underwent Lu-Hf isotopic characterization. The Lu-Hf isotopic analysis of eight grain features is shown in Table 3. In the Hancheng sample, three detrital zircons (3.48%, n = 86) yield 550–360 Ma. The majority of these grains preserve

well-defined oscillatory zoning textures, diagnostic of primary magmatic crystallization processes. Three individual zircon crystals were from the Shihezi Fm, and the Lu-Hf isotopic analysis of eight grain features is shown in Table 3.

Correlations between zircon age spectra and tectonic events reveal that the Early Paleozoic (550–350 Ma) tectonomagmatic activities in the NQinOB and NQiOB served as sediment sources for adjacent basins. In the NQinOB, magmatic activities during 550–350 Ma recorded crust-mantle interactions during the subduction of the Shangdan Ocean, as evidenced via the $\varepsilon_{Hf}(t)$ values (−27.5 to 14.1 [21]). Notably, the negative $\varepsilon_{Hf}(t)$ values (−17.19 to −10.26) coupled with T_{DM2} ages of 2024–2479 Ma indicate the recycling of ancient crustal materials, such as subducted–exhumed high-pressure continental fragments. The high proportion (31.06%) of 550–350 Ma zircons in the Hancheng sample aligns with the erosional history of NQinOB, following its Late Paleozoic uplift, further confirming its role as a primary provenance. Meanwhile, in the NQiOB, Early Paleozoic (~500 Ma) magmatic zircons exhibit a wide $\varepsilon_{Hf}(t)$ range (−5.6 to 12.3), and the slab breakoff event at ~450 Ma during oceanic subduction–collisions triggered asthenospheric upwelling, promoting the generation of hybrid crust–mantle magmas [47] (marked by increased positive $\varepsilon_{Hf}(t)$ values). The zircon age spectra (550–350 Ma) and Hf isotopic signatures (e.g., T_{DM2} age distributions) of the Luonan sample closely resemble those of the NQiOB, suggesting a shared provenance linkage. Specifically, the $\varepsilon_{Hf}(t)$ values (−41 to 13) and T_{DM2} age spans (596–3940 Ma) of 550–350 Ma zircons in Luonan reflect dual contributions from the recycled TNCO basement and mantle-derived materials. The positive $\varepsilon_{Hf}(t)$ values (0.1–13.0) and younger T_{DM2} ages (596–1410 Ma) correlate with crust-mantle hybridization processes in the NQiOB. In contrast, Hancheng zircons of the same age group exclusively display negative $\varepsilon_{Hf}(t)$ values (−17.19 to −10.41) and T_{DM2} ages (2024–2479 Ma). These spatioisotopic correlations collectively demonstrate that the subduction-exhumation dynamics of the NQinOB and the collisional-extensional mechanisms of the NQiOB jointly governed the sediment supply patterns to the southern margin of the TNCO during the Early Paleozoic. Although the Late Paleozoic detrital zircons from the Alxa region exhibit age spectrum peaks around 420 Ma that correspond to those observed in the Luonan and Hancheng areas (Figure 10i), their distinct geochemical signatures preclude a major provenance relationship. The Alxa Late Paleozoic zircons are predominantly characterized by juvenile crustal sources ($\varepsilon_{Hf}(t) > 0$) (Figure 11a), whereas those from Luonan–Hancheng display clear evidence of ancient crustal recycling ($\varepsilon_{Hf}(t) < 0$). This fundamental discrepancy in crustal evolution mechanisms, with Alxa demonstrating significant juvenile crustal input versus Luonan–Hancheng dominant ancient crustal reworking, reveals incompatible provenance processes. Therefore, it is concluded that the Alxa region was not a dominant provenance relative to the Luonan–Hancheng detrital provenances.

Based on previous U-Pb geochronological results, magmatic events in the NQinOB with ages ranging from 500 Ma to 400 Ma are further subdivided into three peaks as follows: 424 Ma, 451 Ma, and 484 Ma [47] (Figure 10g). This corresponds to the following distinct tectonic regimes: ~500 Ma, deep continental subduction; ~450 Ma, crustal thickening and uplift triggered by continent-continent collision; ~420 Ma, post-collisional crustal uplift. The Hf isotopic compositions of the NQinOB exhibit significant heterogeneity, as follows: $\varepsilon_{Hf}(t)$: −27.6 to 14.6 (mean: −2.1); and T_{DM2}: 551–2759 Ma (mean: 1398 Ma). Notably, ~80% of T_{DM2} values cluster below 2.0 Ga (Figure 11a,b). This indicates the reworking of the Neoarchean–Neoproterozoic crust. By 500 Ma, most magmatic zircons had negative $\varepsilon_{Hf}(t)$ values, suggesting that they were primarily derived from reworked continental crust. A small fraction of zircons exhibited positive $\varepsilon_{Hf}(t)$ values, indicating the involvement of mantle-derived magmas. Subsequently, the NQinOB geological body underwent two phases of back-arc uplift, transitioning toward a stretching environment.

During this period, the positive zircon $\varepsilon_{Hf}(t)$ values significantly increased (Figure 11a), and thus, magmatic activity since 450 Ma has been characterized by a wide range of zircon $\varepsilon_{Hf}(t)$ values, reflecting a crust-mantle magma mixing signature. Overall, the T_{DM2} of the NQinOB mainly ranges from 0.6 Ga to 2.5 Ga (Figure 11b). In addition, the 517–324 Ma metamorphism ages have also been reported (Figure 10g). The NQinOB records polyphase metamorphism spanning 500–420 Ma, with subordinate thermal events persisting into the Carboniferous period (<350 Ma) [48,49] (Figure 10g).

In the Permian period, zircon populations defining two age clusters (512–380 Ma and 350–256 Ma) exhibit predominantly negative $\varepsilon_{Hf}(t)$ values, correlating with Paleoproterozoic T_{DM2} model ages (1.97–1.72 Ga) and (2.4–1.6 Ga) Ma, respectively [50]. The late Paleozoic Permian strata of the SQinOB are derived from the southern margin of the TNCO and the NQinOB. The age group of approximately 260–380 Ma in the Permian sediments of the SQinOB is similar to the age data from the TNCO, suggesting that the NQinOB experienced an uplift before the late Permian.

(4) Late Paleozoic (350–260 Ma)

In the Luonan sample, 40 detrital zircon grains (20.51%, n = 95) fall within the 350–260 Ma age range. The Lu-Hf isotopic analysis of eight grain features is shown in Table 3. This signature is likely linked to post-collisional extensional magmatism along the southern margin of the TNCO during 350–260 Ma.

In the Hancheng sample, 14 detrital zircons (16.27%, n = 86) yield 350–260 Ma. Most of them show typical magmatic zircon features. Within the 350–260 Ma population (12 grains), the Lu-Hf isotopic analysis of 8 grain features is shown in Table 3. It is similar to the zircons of the same period in Luonan, but the proportion is significantly lower, and it is probably controlled by regional tectonic differences.

Previous studies have identified a group of metamorphic zircons with a U-Pb weighted average age of 342 Ma in the intrusions of the Wuguan pluton in Danfeng County, eastern NQinOB. These zircons are interpreted to reflect a tectonothermal event in the region occurring after 438 Ma [51]. Other scholars suggest that around 350 Ma, there may have been a tectonothermal event in the NQinOB [52]. Metamorphic stratigraphic studies in the NQinOB suggest that the NQinOB experienced an intense tectonothermal event during the Permian–Triassic (280–240 Ma), which led to regional metamorphism. The 350–260 Ma detrital zircons from the southern Ordos Basin margin exhibit provenance signatures analogous to those reported in the Qinling Orogenic Belt, corroborating its role as a dominant source region during this interval. We propose that the ca. 350–260 Ma detrital zircons in the Zhen'an Basin of the SQinOB originated from the NQinOB, possibly sharing the same source as the detrital zircons of this age in the Shihezi Fm of the southern Ordos Basin, and they do not derive from the southern margin of the TNCO near Luonan.

Permian successions record two distinct detrital zircon populations (512–380 Ma and 350–256 Ma), and they have predominantly negative $\varepsilon_{Hf}(t)$ signatures, yielding the following: T_{DM2}: 1968–1720 Ma and 2484–1668 Ma, respectively [50]. The late Paleozoic Permian sediments of the SQinOB are primarily derived from the southern margin of the TNCO and the NQinOB. The age group of approximately 260–380 Ma in the Permian sediments of the SQinOB is similar to the age data from the TNCO, suggesting that the NQinOB experienced an uplift before the Late Permian. Therefore, the 350–260 Ma provenance of the Shihezi Fm in Luonan and Hancheng is from the SQinOB. Although the age histograms of Luonan and Hancheng at 350–260 Ma have similar peaks to those of Yinshan (Figure 10k), the T_{DM2} ages of 350–260 Ma zircons from the Luonan–Hancheng area are significantly higher than those of the Yinshan region (2.4–3.0 Ga vs. <1.5 Ga), indicating distinct crustal evolutionary histories in their source regions and further supporting that the Yinshan region was not a major provenance [21].

5.4. Comprehensive Provenance Analysis of the Shihezi Formation

Integrated analyses combining assemblage characteristics with standardized indices (ATi, GZi, etc.) were employed to decipher heavy mineral provenance signatures and assemblage types, and the spatial distribution patterns of the Shihezi Fm in Luonan (North China Block) exhibit significant similarities to those of the Shihezi Fm in Hancheng (southern Ordos Basin). The quantitative analysis of heavy mineral indices reveals that the ZTR index (zircon-tourmaline-rutile index) in Hancheng exceeds that of Luonan, suggesting a progressive diminution in stable heavy mineral content and sediment maturity from Hancheng to Luonan. Furthermore, higher ATi index (apatite-tourmaline index) and GZi index (garnet-zircon index) values in the Hancheng samples imply dominant sediment derivation from intermediate-acidic igneous rocks, with limited supply from low-grade to medium-grade metamorphic source rocks. These findings collectively demonstrate systematic provenance differentiation between the Luonan and Hancheng depositional systems. Combined with the paleocurrent of Han Cheng by previous authors, we believe that the material sources of Han Cheng came from TNCO, NQinOB, and NQiOB.

Based on the geochemical analyses of Luonan and Hancheng, the provenance of Luonan is primarily sourced from the Proterozoic basement of the southern TNCO. Its tectonic setting corresponds to a stable craton, consistent with the foreland basin sedimentary system of the Qinling Orogenic Belt. Felsic source rocks dominate the provenance of Hancheng but incorporate minor intermediate-mafic components (e.g., Late Paleozoic metamorphosed mafic rocks or intermediate-felsic volcanic rocks from the Qinling Orogenic Belt). Its tectonic setting reflects an active continental margin influenced by Mesozoic tectonic-magmatic activity (e.g., reactivation of the southern TNCO). The provenance of Luonan–Hancheng records a transition from a stable craton (Luonan) to a tectonically reactivated zone (Hancheng) along the southern TNCO margin, and this is likely linked to the Late Mesozoic post-collisional extension of the Qinling Orogenic Belt.

For sample HC-01 from the Shihezi Fm of Hancheng, the majority of Phanerozoic detrital zircons have negative $\varepsilon_{Hf}(t)$ values (Figure 11a), with only one zircon showing a positive $\varepsilon_{Hf}(t)$ value, and T_{DM2} ranging from 2.7 to 1.2 Ga (Figure 11b). For sample LN-20 from the Shihezi Fm of Luonan, most Phanerozoic detrital zircons display 16 positive $\varepsilon_{Hf}(t)$ values, with T_{DM2} between 409 Ma and 2941 Ma. At the same time, 15 portions show negative values, with T_{DM2} between 1473 Ma and 3940 Ma, indicating a significant addition of new crustal material. Sample LN-03 has negative $\varepsilon_{Hf}(t)$ values for all Phanerozoic detrital zircons, with T_{DM2} between 2.5 Ga and 1.5 Ga, and it does not show a notable addition of new crustal material as the zircon originates from an older continental crust. The zircon ages, Hf isotopic compositions, and T_{DM2} of samples LN-03 and HC-01 are similar. According to previous studies, the paleocurrent study in Hancheng suggests that the source of the sedimentary material is from the southwestern, southern, and southeastern marginal orogenic belts of the basin, specifically from the northern Qinling direction, rather than from the source region of the northern Xingmeng orogenic belt. Therefore, we infer that the provenance of sample LN-03 also comes from the NQinOB. Due to the collision and orogenic movement between the Central Asian Orogenic Belt and the northern margin of the TNCO, intense magmatic activity occurred in the Xingmeng Orogenic Belt during ca. 350–250 Ma. The ca. 350–260 Ma detrital zircon population identified within the Shihezi Fm (northern Ordos Basin) has been proposed to correlate with magmatic sources in the Xing–Meng Orogenic Belt based on isotopic and provenance linkage studies [53]. With the integrated analysis of prior studies, it is proposed that the southern and northern domains of the Ordos Basin have different source supplies. Given that the Hf isotopic characteristics of Hancheng and Luonan are similar, we conclude that the Xingmeng Orogenic Belt did not supply the source for the Luonan region. Sample LN-20 contains three young zircons ages

comprising 287 Ma, 300 Ma, and 322 Ma, and a Th/U < 0.1, characteristic of metamorphic zircons. This suggests the presence of an important, yet underrecognized, tectonic and thermal event in theNQinOB or/and NQiOB during ca. 350–260 Ma.

In summary, the Luonan strata were derived from the Archean–Paleoproterozoic basement of the TNCO and Late Paleozoic post-collisional magmatic rocks. The Luonan area represents a long-term stable southern cratonic margin influenced by the Late Paleozoic exhumation processes of the Qinling Orogenic Belt. In contrast, the Hancheng materials originated from mixed sources of the TNCO basement and NQinOB Paleoproterozoic–Early Paleozoic metamorphic rocks, reflecting its tectonic setting within a transitional zone between the craton and orogenic belt, controlled by the multiphase activities of the NQinOB. Based on the heavy mineral assemblages, geochemical signatures, and isotopic characteristics, distinct provenance differences between Luonan and Hancheng reveal a tectonic transition from a stable craton (Luonan) to the active orogenic belt (Hancheng) along the southern TNCO margin. This transition correlates with multiple collisional-exhumation-extension cycles of the Qinling Orogenic Belt. Notably, the Hancheng samples analyzed in this study exhibit similar heavy mineral characteristics and U-Pb age spectra to those reported in [47], while maintaining partial similarities with Luonan sample. These observations collectively suggest a shared provenance for the Shihezi Fm deposits in both the Hancheng and Luonan regions.

Previous studies proposed that the Inner Mongolia Uplift also served as a provenance for the Luonan area, and the Late Paleozoic magmatic rocks (390–237 Ma) are from the YB [7]. These zircons record tectonic uplift and magmatic activities associated with subduction during the Late Paleozoic. The uplift and denudation of the YB supplied Late Paleozoic detrital zircons to the strata of the TNCO. The southward extension of the Shihezi Fm deltaic system and the north-to-south paleocurrent directions in the TNCO were interpreted as evidence supporting the Inner Mongolia Uplift as a provenance. However, our paleocurrent measurements from the Hancheng Shihezi Fm show W and NW [21], implying provenance contributions from the southeastern and eastern regions. Heavy mineral assemblages and geochemical signatures reveal that the rare earth element (REE) distribution patterns of Luonan and Hancheng are consistent with the ancient basement of the TNCO. Notably, the stable cratonic setting of Luonan contrasts sharply with the active continental margin or collisional tectonic affinity of the Inner Mongolia Uplift. The elevated Th/Co ratios in Luonan sediments differ significantly from the mafic-dominated provenance signature of the Inner Mongolia Uplift. In Hancheng, the intermediate-mafic components likely originated from the NQinOB rather than the distal and tectonically distinct Inner Mongolia Uplift. Based on sediment geochemistry, we conclude that the Luonan provenance is primarily derived from the TNCO with secondary contributions from the NQinOB, while Hancheng sediments reflect a hybrid source dominated by the TNCO and NQinOB. The intermediate-mafic components in Hancheng may originate from Late Paleozoic magmatic and/or metamorphic events in the NQinOB. Although detrital zircon age spectra from Luonan include peaks corresponding to Permian magmatism in the Inner Mongolia Uplift, Lu-Hf isotopic analyses ($\varepsilon_{Hf}(t) < 0$ of the Luonan and Hancheng) align more closely with ancient cratonic basement recycling (TNCO) rather than juvenile crustal inputs ($\varepsilon_{Hf}(t) > 0$) characteristic of the Inner Mongolia Uplift.

5.5. Tectonic Implications

Based on the heavy mineral assemblages, characteristic indices of heavy minerals, sedimentary geochemical characteristics, and isotopic analyses, it can be inferred that the Hancheng and Luonan regions share identical provenances. This conclusion sufficiently demonstrates that Luonan belonged to the southern margin of the TNCO (Figure 12)

during the deposition of the Shihezi Fm. However, it was subsequently incorporated into the Qinling mountain system during the uplift and orogenic processes of the Qinling Orogenic Belt. The tectonic affinity of Luonan thus remains fundamentally attached to the southern margin of the TNCO. Scholars previously believed that the intensity of tectonic uplift in the NQiOB was higher than that in the NQinOB, and that the NQinOB and the NQiOB provided sources for the southern part of the Ordos Basin and were the basis for the collision of the Permian System of the North China Plate [8]. Furthermore, the presence of 260–350 Ma detrital zircon ages in Luonan suggests potential contributions from southern source regions. Nevertheless, current geological records from the Qinling Orogenic Belt exhibit limited evidence of intensive tectonothermal events corresponding to this specific zircon age window, which necessitates further investigation into regional magmatic-tectonic evolution and provenance discrimination.

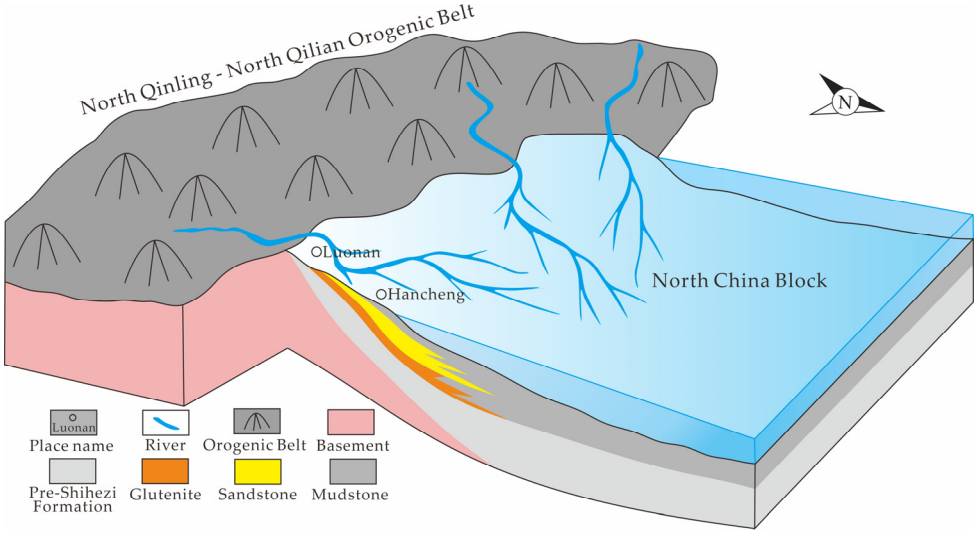


Figure 12. Schematic diagram of the tectonic evolution of the North Qinling–North Qilian Orogenic Belts and the North China Craton. Plotted with CorelDRAW Graphics Suite 2021 software, version 23.5.0.506.

Within the Qinling Orogenic Belt, the scattered ca. 350–260 Ma area presents reliable records of magmatic-metamorphic zircon ages and a large number of records of disputed zircon ages [52,54–59]. However, methodological limitations constrain the reliability of these age determinations, which remain highly debated in current research. Significant discrepancies in Permian paleocurrent directions, heavy mineral assemblages, detrital zircon age spectra, Lu-Hf, and T_{DM2} are observed between the southern and northern Ordos Basin, indicating distinct sediment provenances between these two regions [42]. Notably, NQinOB could potentially serve as a provenance contributor for the ca. 350–260 Ma zircon components in the southern Ordos Basin. Furthermore, the Permian sedimentary sequences within the Qinling Orogenic Belt exhibit zircon age spectra, Hf isotopic signatures, and two-stage model ages that are strikingly similar to those of the southern Ordos Basin [21,27,41,50,60–62]. These collective observations suggest that the Qinling Orogenic Belt and the Ordos Basin had already undergone collisional orogenesis during the Permian, establishing the orogen as a critical sediment source for adjacent basins.

The findings demonstrate that the ca. 350–260 Ma detrital zircons in the Permian strata of the southern Ordos Basin and Qinling Orogenic Belt share a common provenance, predominantly derived from the Qinling Orogenic Belt rather than the previously proposed Yinshan Block or Alxa Block. If subsequent studies confirm that the ca. 350–260 Ma detrital zircons in the Middle–Upper Permian sequences of the southern Ordos Basin, Liuyehe Basin, Lintan area, and Zhen'an Basin indeed originate from the Qinling Orogenic Belt (as

preliminarily supported by existing data), this conclusion would carry significant theoretical and practical implications. First, it would provide critical constraints for reconstructing the Late Paleozoic tectonic evolution and plate affinity of the Qinling Orogenic Belt, clarifying the spatiotemporal controls of its orogenic processes on sedimentary filling in adjacent basins. Second, it would substantially address current knowledge gaps regarding Late Paleozoic tectonothermal events in the Qinling Orogenic Belt. Furthermore, this discovery would not only refine the provenance discrimination of ca. 350–260 Ma detrital zircons in the southern margin of the TNCO but also establish a new framework for investigating the far-field tectonic interactions between the Central Asian Orogenic Belt, the Qinling Orogenic Belt, and the TNCO during subduction-collisional orogenesis.

During the Late Carboniferous to Late Permian, the northward subduction of the Mianlue Ocean provided the driving force for the tectonic uplift and exhumation of the NQinOB [63–65], which subsequently became a critical sediment source for peripheral basins. However, the current geological record within the Qinling Orogenic Belt reveals scarce reliable magmatic-metamorphic zircon ages of ca. 350–260 Ma (only sporadic credible ages have been reported in the NQinOB and West Qinling Orogenic Belt, while most other regions exhibit highly debated age data). This scarcity may be attributed to a combination of factors as follows: (1) the tectonothermal events during this interval likely generated limited volumes of igneous-metamorphic rocks; (2) these rocks were extensively eroded during the subsequent multi-phase uplift of the Qinling Orogenic Belt or obscured by later magmatic events. Consequently, we propose that the NQinOB experienced an episode of intense tectonothermal activity at 260–350 Ma, which has been previously overlooked. This event likely reflects dynamic processes driven by the evolving subduction of the Mianlue Ocean system.

6. Conclusions

(1) The heavy mineral composition, assemblage types, and spatial distribution of the Shihezi Fm in Luonan and Hancheng exhibit a high degree of similarity. Geochemical analyses reveal that Luonan provenance mainly originated from the stable margin of the TNCO, with additional input from the materials of an active orogenic belt. In contrast, the Hancheng provenance demonstrates tectonic settings characteristic of continental magmatic arcs and active continental margins, which are suggested to be linked to subduction events associated with the NQinOB. This evidence indicates that NQinOB–NQiOB collectively constitute the provenance system for these regions.

(2) The detrital zircon age spectra and Hf isotopic signatures of Luonan and Hancheng exhibit remarkable similarity, and 2600–1600 Ma zircons were derived from the TNCO basement. Zircons spanning ~1.0–0.5 Ga (979–550 Ma) dominantly reflect the North Qinling Orogenic Belt as their protolith source region, 550–340 Ma zircons were sourced from the North Qinling Orogenic Belt, and 350–260 Ma zircons were sourced from either the North Qinling Orogenic Belt or/and the North Qilian Orogenic Belt.

(3) Comprehensive provenance analyses show that the provenance of the Shihezi Formation in Luonan and Hancheng are partially similar, with the TNCO basement as the core provenance, followed by Paleozoic collision-related regenerated materials in Luonan; Hancheng is significantly superimposed with respect to the contribution of NQinOB.

(4) The Qinling Orogenic Belt experienced a significant tectonothermal event during ca. 350–260 Ma. This tectonothermal episode served as the principal source for the 350–260 Ma detrital materials deposited in Luonan and Hancheng.

Supplementary Materials: The following supporting information can be downloaded at: https://www.mdpi.com/article/10.3390/min15050549/s1, Table S1: Major element data from the Shihezi

Formation sandstones in Luonan and Hancheng; Table S2: Trace element data from the Shihezi Formation sandstones in Luonan and Hancheng; Table S3: Zircon LA-ICP-MS U-Pb isotope data from the Shihezi Formation sandstones in Luonan and Hancheng; Table S4: Lu-Hf isotope data from the Shihezi Formation in Luonan and Hancheng.

Author Contributions: Data curation, X.Z., Z.Z., Z.L. and W.Z.; Writing—original draft, Y.D. (Yuliang Duan), W.P. and L.M.; Writing—review and editing, Y.D. (Yuliang Duan), W.P. and Z.J.; Supervision, Y.D. (Yi Ding) and W.L. All authors have read and agreed to the published version of the manuscript.

Funding: This research is funded by the National Natural Science Youth Fund Project (41702117), National Natural Science Key Fund Project (41330315), China Geological Survey Mineral Resources Investigation and Evaluation Project (121201011000150014) "Fundamental Geological Investigation of Oil and Gas in Ordos Peripheral Basin Group"; the National Nature Science Foundation of China (No. 42002004), Scientific Research Program Funded by Shaanxi Provincial Education Department (No. 22JK0374), Talent Fund of Weinan Normal University (No. 2021RC28); and the Qinghai University Youth Research Fund Project (2021-QGY-8).

Data Availability Statement: Data are available upon request to the corresponding author of the manuscript.

Conflicts of Interest: Yuliang Duan was employed by the company Yanchang Oilfield Co., Ltd., Xi Zhang was employed by the company PetroChina Changqing Oilfield Co., Ltd., Zhengtao Zhang and Zhichao Li were employed by the company PetroChina Changqing Oilfield Co., Ltd. The remaining authors declare that the research was conducted in the absence of any commercial or financial relationships that could be construed as a potential conflict of interest.

References

1. Yang, H.T.; Liu, X.W.; Xue, Y.S. Zircon LA-ICP-MS U-Pb ages and geochemical characteristics of the Changling alkaline complex in Luonan County, Shaanxi Province, northwest China. *Min. Resour. Geol.* **2019**, *33*, 287–295. (In Chinese with English Abstract)
2. Chen, H.; Zhang, C.; Liu, X.; Dong, Y.; Tan, X.; Chen, Q.; Zhang, Z.; Wei, K. Detrital zircon U-Pb geochronology and provenance of Silurian, Devonian and Permian sedimentary rocks, South Qinling: Constraints on late Palaeozoic tectonic evolution history of the Qinling Orogenic Belt. *Geol. J.* **2023**, *59*, 811–837. [CrossRef]
3. Huang, J.W. Geochronology and Geochemistry of the Qinling Complex and Shahewan, Caoping Granites in South Qinling and Their Significance. Master's Thesis, Guilin University of Technology, Guilin, China, 2019. (In Chinese with English Abstract)
4. Cao, H.; Li, S.; Zhao, S.; Yu, S.; Li, X.; Somerville, I. Detrital zircon geochronology of Neoproterozoic to early Paleozoic sedimentary rocks in the North. Qinling Orogenic Belt: Implications for the tectonic evolution of the Kuanping Ocean. *Precambrian Res.* **2016**, *279*, 1–16. [CrossRef]
5. Wang, M.Y. The Petrological and Geochemical Study of Syenite in Changling of Luonan County, Shaanxi Province. Master's Thesis, China University of Geosciences, Beijing, China, 2016. (In Chinese with English Abstract)
6. Fang, T. Sediment Provenance Characteristics and Uplift Process of Permian in Southern Margin of North China. Master's Thesis, Henan University of Science and Technology, Luoyang, China, 2023. (In Chinese with English Abstract)
7. Yang, W.; Fang, T.; Wang, Y.; Sha, H. Late Paleozoic Tectonic Evolution of the Qinling Orogenic Belt: Constraints of Detrital Zircon U-Pb Ages from the Southern Margin of North China Block. *Minerals* **2022**, *12*, 864. [CrossRef]
8. Zhu, S.Y.; Liu, L.; Wang, L.L.; Wang, Z.W.; Hu, J.L.; Zhang, J.Q.; Zhang, C.G.; Zhao, J.X.; Chen, H.D. Provenance signature and tectono–sedimentary setting of the Permian Shihezi formation (Ordos basin, China): Insights from geochemistry and detrital zircon U–Pb dating. *Mar Pet. Geol.* **2024**, *165*, 106901. [CrossRef]
9. Reng, J.F. Paleozic Tectonic Transformation of the North Qinling Belt in Shanxi Province. Master's Thesis, Northwest University, Xi'an, China, 2004.
10. Peng, Z.H.; Peng, S.M.; Wu, Z.H. Basin pattern and evolution of Triassic in North China. *J. Xi'an Shiyou Univ. (Nat. Sci. Ed.)* **2009**, *24*, 34–38+4. (In Chinese with English Abstract)
11. Chen, G.; Li, Y.; Han, W.; Niu, Y.; Zhang, Q. Discussion on sandstone characteristic and provenance of Permian Shihezi Formation in Luonan, Shaanxi Province. *Chin. J. Geol.* **2020**, *55*, 1001–1011. [CrossRef]
12. Chen, A.; Chen, H.-D.; Xiang, F.; Liu, W.-J.; Hou, Z.; Shang, Y.-Z.; Ye, L.-M.; Li, J. Sandstone characteristic and provenance analysis of the Permian Shanxi Formation-Shangshihezi Formation in the northeast of Ordos Basin, China. *J. Chengdu Univ. Technol. (Sci. Technol. Ed.)* **2007**, *48*, 305–311. (In Chinese with English Abstract)

13. Zhang, C.; Diwu, C.; Kröner, A.; Sun, Y.; Luo, J.; Li, Q.; Gou, L.; Lin, H.; Wei, X.; Zhao, J. Archean-Paleoproterozoic crustal evolution of the Ordos Block in the North China Craton: Constraints from zircon U–Pb geochronology and Hf isotopes for gneissic granitoids of the basement. *Precambrian Res.* **2015**, *267*, 121–136. [CrossRef]
14. Dong, Y.; Zhang, X.; Liu, X.; Li, W.; Chen, Q.; Zhang, G.; Zhang, H.; Yang, Z.; Sun, S.; Zhang, F. Propagation tectonics and multiple accretionary processes of the Qinling Orogen. *J. Asian Earth Sci.* **2015**, *104*, 84–98. [CrossRef]
15. Liu, S.; Su, S.; Zhang, G. Early Mesozoic basin development in North China: Indications of cratonic deformation. *J. Asian Earth Sci.* **2013**, *62*, 221–236. [CrossRef]
16. Morton, A.C.; Hallsworth, C. Identifying provenance-specific features of detrital heavy mineral assemblages in sandstones. *Sediment. Geol.* **1994**, *90*, 241–256. [CrossRef]
17. Zhao, J. The Paleoproterozoic Tectonic Evolution of the Central Segment of the North China Craton–Constrained by Magmatic and Metamorphic Records of Lüliang Complex. Ph.D. Thesis, Northwest University, Xi'an, China, 2018. (In Chinese with English Abstract)
18. Liu, Y.; Liu, X.; Hu, Z.; Diwu, C.; Yuan, H.-L.; Gao, S. Evaluation of accuracy and long-term stability of determination of 37 trace elements in geological samples by ICP-MS. *Acta Petrol. Sin.* **2007**, *23*, 1203–1210. (In Chinese with English Abstract)
19. Gong, W. Provenance Analysis and Detrital Zircon U-Pb Dating of Chang 6 and Chang 4+5 of Yanchang Formation in Dingbian and Xiasiwan Area, Ordos Basin. Master's Thesis, Northwest University, Xi'an, China, 2022. [CrossRef]
20. Ludwig, K.R. User's manual for isoplot 3.00, a geochronlogical toolkit for microsoft excel. *Berkeley Geochronl. Cent. Spec. Publ.* **2003**, *4*, 25–32.
21. Jiang, Z.W. The Study of Provenance and Basin Mountain Coupling of Shan1-H8 Member, Upper Palaeozoic, Southern Ordos Basin. Ph.D. Thesis, Northwest University, Xi'an, China, 2020. (In Chinese with English Abstract)
22. Blichert-Toft, J.; Albarède, F. The Lu-Hf isotope geochemistry of chondrites and the evolution of the mantle-crust system. *Earth Planet. Sci. Lett.* **1997**, *148*, 243–258. [CrossRef]
23. Griffin, W.L.; Pearson, N.; Belousova, E.; Jackson, S.; van Achterbergh, E.; O'reilly, S.Y.; Shee, S. The Hf isotope composition of cratonic mantle: LAM-MC-ICPMS analysis of zircon megacrysts in kimberlites. *Geochim. Cosmochim. Acta* **2000**, *64*, 133–147. [CrossRef]
24. Söderlund, U.; Patchett, P.J.; Vervoort, J.D.; Isachsen, C.E. The 176Lu decay constant determined by Lu-Hf and U–Pb isotope systematics of Precambrian mafic intrusions. *Earth Planet. Sci. Lett.* **2004**, *219*, 311–324. [CrossRef]
25. Amelin, Y.; Lee, D.-C.; Halliday, A.N.; Pidgeon, R.T. Nature of the Earth's earliest crust from hafnium isotopes in single detrital zircons. *Nature* **1999**, *399*, 252–255. [CrossRef]
26. Wu, F.Y.; Li, X.H.; Zheng, Y.E.; Gao, S. Lu-Hf isotopic systematics and their applications in petrology. *Acta Petrol. Sin.* **2007**, *23*, 185–220. (In Chinese with English Abstract)
27. Jiang, Z.; Luo, J.; Liu, X.; Hu, X.; Ma, S.; Hou, Y.; Fan, L.; Hu, Y. Provenance and Implication of Carboniferous–Permian Detrital Zircons from the Upper Paleozoic, Southern Ordos Basin, China: Evidence from U-Pb Geochronology and Hf Isotopes. *Minerals* **2020**, *10*, 265. [CrossRef]
28. Wu, C.D.; Lin, C.S.; Shen, Y.P.; Fen, X. Characteristics of the fractions and heavy mineral assemblages of the Jurassic sandstones of the Kucha depression and their source-area properties. *Prog. Nat. Sci.* **2005**, *15*, 37–43. (In Chinese)
29. Morton, A.C.; Hallsworth, C.R. Processes controlling the composition of heavy mineral assemblages in sandstones. *Sediment. Geol.* **1999**, *124*, 3–29. [CrossRef]
30. Wang, Q.L.; Hu, S.H.; Li, C.A. Heavy mineral characteristics of gravel layers in the Zhoulao Town borehole. *Geol. China* **2009**, *36*, 878–884. (In Chinese with English Abstract)
31. Yang, G.J.; Wu, K.Y.; Zhang, B.C. Application of U-Pb isotopic dating and heavy mineral assemblage to source-sink system analysis of the Paleogene in western margin of Qaidam Basin. *Mar. Petro Geol.* **2024**, *29*, 269–279. (In Chinese with English Abstract)
32. Taylor, S.R.; Mclennan, S.M. *The Continental Crust: Its Composition and Evolution, An Examination of the Geochemical Record Preserved in Sedimentary Rocks*; Blackwell Scientific Publishing: Oxford, UK, 1985; pp. 117–140.
33. Rudnick, R.; Gao, S. The role of lower crustal recycling in continent formation. *Geochim. Cosmochim.* **2003**, *67*, 403.
34. Sun, S.S.; McDonough, W.F. Chemical and isotopic systematics of oceanic basalts: Implications for mantle composition and processes. In *Magmatism in the Ocean Basins*; Geological Society Special Publication: London, UK, 1989; Volume 42, pp. 313–345. [CrossRef]
35. Nesbitt, H.W.; Young, G.M. Early Proterozoic climates and plate motions inferred from major element chemistry of lutites. *Nature* **1982**, *299*, 715–717. [CrossRef]
36. Mclennan, S.M.; Hemming, S.; McDaniel, D.K.; Hanson, G.N. Geochemical approaches to sedimentation, provenance, and tectonics. In *Processes Controlling the Composition of Clastic Sediments*; Geological Society of America: New York, NY, USA, 1993. [CrossRef]

37. Panahi, A.; Young, G.M.; Rainbird, R.H. Behavior of major and trace elements (including REE) during Paleoproterozoic pedogenesis and diagenetic alteration of an Archean granite near Ville Marie, Québec, Canada. *Geochim. Cosmochim.* **2000**, *64*, 2199–2220. [CrossRef]
38. Roser, B.P.; Korsch, R.J. Determination of tectonic setting of sandstone-mudstone suites using SiO_2 content and K_2O/Na_2O ratio. *J. Geol.* **1986**, *94*, 635–650. [CrossRef]
39. Roser, B.P.; Korsch, R.J. Provenance signatures of sandstone-mudstone suites determined using discriminant function analysis of major-element data. *Chem. Geol.* **1988**, *67*, 119–139. [CrossRef]
40. Bhatia, M.R.; Crook, K.A.W. Trace element characteristics of graywackes and tectonic setting discrimination of sedimentary basins. *Contrib. Mineral. Petrol.* **1986**, *92*, 181–193. [CrossRef]
41. Cheng, C. The Evolution of Permian Sedimentary Sequences in Zhen'an, Shananxi, China, and Its Response to the Changes of Permian Paleoclimate, Paleoenviroment and Paleogeography. Ph.D. Thesis, Hefei University of Technology, Hefei, China, 2018. [CrossRef]
42. Zhou, Z.-J.; Mao, S.-D.; Chen, Y.-J.; Santosh, M. U–Pb ages and Lu–Hf isotopes of detrital zircons from the southern Qinling Orogen: Implications for Precambrian to Phanerozoic tectonics in central China. *Gondwana Res.* **2016**, *35*, 323–337. [CrossRef]
43. Pan, W.; Jiang, Z.; Fan, L.; Zhang, Z.; Li, Z.; Ma, S.; Wang, Z.; Li, X.; Zhao, W. Provenance of the He 8 Member of the Upper Paleozoic Shihezi Formation, Ordos Basin, China: Insights from Heavy Minerals, Paleocurrents, Detrital Zircon Chronology, and Hf Isotopes. *Minerals* **2024**, *14*, 1076. [CrossRef]
44. Meng, E.; Xu, W.-L.; Pei, F.-P.; Yang, D.-B.; Yu, Y.; Zhang, X.-Z. Detrital-zircon geochronology of Late Paleozoic sedimentary rocks in eastern Heilongjiang Province, NE China: Implications for the tectonic evolution of the eastern segment of the Central Asian Orogenic Belt. *Tectonophysics* **2010**, *485*, 42–51. [CrossRef]
45. Wang, F.; Xu, W.-L.; Gao, F.-H.; Zhang, H.-H.; Pei, F.-P.; Zhao, L.; Yang, Y. Precambrian terrane within the Songnen–Zhangguangcai Range Massif, NE China: Evidence from U–Pb ages of detrital zircons from the Dongfengshan and Tadong groups. *Gondwana Res.* **2014**, *26*, 402–413. [CrossRef]
46. Cui, K. Provenance of the Upper Paleozoic Shan1-He 8 Formation in Southern Ordos Basin and Its Influence on the Sedimentary Filling Pattern. Master's Thesis, Northwest University, Xi'an, China, 2019. (In Chinese with English Abstract)
47. Zhang, C.L.; Liu, L.; Wang, T. Granitic magmatism related to early Paleozoic continental collision in North Qinling. *Sci. Bull.* **2013**, *58*, 4405–4410. [CrossRef]
48. Liu, L. Multi-matemorphic timings of HP-UHP rocks in the North Qinling and their geological implications. *Acta Petrol. Sin.* **2013**, *29*, 1634–1656. (In Chinese with English Abstract)
49. Liu, L.; Liao, X.; Wang, Y.; Wang, C.; Santosh, M.; Yang, M.; Zhang, C.; Chen, D. Early Paleozoic tectonic evolution of the North Qinling Orogenic Belt in Central China: Insights on continental deep subduction and multiphase exhumation. *Earth-Sci. Rev.* **2016**, *159*, 58–81. [CrossRef]
50. Cheng, C.; Li, S.; Xie, X.; Manger, W.L.; Busbey, A.B. U–Pb detrital zircon geochronology and Hf isotopic composition of Permian clastic rocks, Zhen'an basin, South Qinling belt: Implications for the Paleozoic tectonic evolution of the Qinling orogenic belt. *Int. Geol. Rev.* **2019**, *61*, 1462–1478. [CrossRef]
51. Li, P.; Chen, J.L.; Xu, X.Y. Petrogenesis and LA-ICPMS zircon U-Pb dating of the Wuguan intrusive body in North Qinling. *Acta Petrol. Miner.* **2011**, *30*, 610–624. (In Chinese with English Abstract)
52. Li, Y.; Zhou, H.; Li, Q. Palaeozoic polymetamorphism in the North Qinling orogenic belt, Central China: Insights from petrology and in situ titanite and zircon U-Pb geochronology. *J. Asian Earth Sci.* **2014**, *92*, 77–91. [CrossRef]
53. Han, H.P.; Wu, C.Y.; Bai, Q.H. Zircon U-Pb Dating of Clastic Sandstone in the Upper Paleozoic from Wushenqi Area, Ordos Basin and Its Geological Significance. *Acta Sedimentol. Sin.* **2014**, *32*, 643–653. [CrossRef]
54. Chen, L.Y.; Liu, X.C.; Qu, W. U-Pb zircon ages and geochemistry of the Wuguan complex in the Qinling orogen, central China: Implications for the late Paleozoic tectonic evolution between the Sino-Korean and Yangtze cratons. *Lithos* **2014**, *192–195*, 192–207. [CrossRef]
55. Yan, Z.; Fu, C.L.; Wang, Z.Q. Late Paleozoic subduction-accretion along the southern margin of the North Qinling terrane, central China: Evidence from zircon U-Pb dating and geochemistry of the Wuguan Complex. *Gondwana Res.* **2016**, *30*, 97–111. [CrossRef]
56. Chen, N.S.; Ba, J.; Zhang, L.; Su, W.; Liu, J.B.; Guo, S. Zircon LA-ICP-MS U-Pb dating of the Wuguan Group, Shangdan fault zone, eastern Qinling, China. *Geol. Bull. China* **2009**, *28*, 556–560. (In Chinese with English Abstract)
57. Jiang, X.J. The Study of Sedimentary Characteristic and Tectonic Setting in Easterm Qinling Orogenic Belt. Ph.D. Thesis, Chinese Academy of Geological Sciences, Beijing, China, 2013. (In Chinese with English Abstract)
58. Xu, X.Y.; Chen, J.L.; Gao, T.; Li, P.; Li, T. Granitoid magmatism and tectonic evolution in northern edge of the Western Qinling terrane. *Acta Petrol. Sin.* **2014**, *30*, 371–389. (In Chinese with English Abstract)
59. Sun, X.P.; Xu, X.Y.; Chen, J.L.; Gao, T.; Li, T.; Li, X.B.; Li, X.Y. Geochemical Characteristics and Chronology of the Jiangligou Granitic Pluton in West Qinling and Their Geological Significance. *Acta Geol. Sin.* **2013**, *87*, 330–342. (In Chinese with English Abstract)

60. Song, D.F.; Xiao, W.J.; Collins, A. Late Carboniferous-early Permian arc magmatism in the southwestern Alxa Tectonic Belt (NW China): Constraints on the late Palaeozoic subduction history of the Palaeo-Asian Ocean. *Geol. J.* **2019**, *54*, 1046–1063. [CrossRef]
61. Song, D.F.; Xiao, W.J.; Windley Brian, F. Provenance and tectonic setting of late Paleozoic sedimentary rocks from the Alxa Tectonic Belt (NW China): Implications for accretionary tectonics of the southern Central Asian Orogenic Belt. *Geol. Soc. Am. Bull.* **2021**, *133*, 253–276. [CrossRef]
62. Song, J.X.; Gong, H.J.; Yao, J.L. U-Pb Dating and Hf Isotopes Analysis of Detrital Zircons of the Shanxi Formation in the Otuokeqi Area, Northwestern Ordos Basin. *Geofluids* **2021**, *2021*, 1–14. [CrossRef]
63. Li, S.G.; Hou, Z.H.; Yang, Y. Timing and geochemical characters of the Sanchazi magmatic arc in Mianlüe tectonic zone, South Qinling. *Sci. China Ser. D Earth Sci.* **2004**, *47*, 317–328. (In Chinese with English Abstract) [CrossRef]
64. Zhang, G.; Dong, Y.; Lai, S.; Guo, A.; Meng, Q.; Liu, S.; Cheng, S.; Yao, A.; Zhang, Z.; Pei, X.; et al. Mianlüe tectonic zone and Mianlüe suture zone on southern margin of Qinling-Dabie orogenic belt. *Sci. China Ser. D Earth Sci.* **2004**, *47*, 300–316. (In Chinese with English Abstract) [CrossRef]
65. Gao, X.Y.; Pei, X.Z.; Li, Z.C.; Li, R.B.; Wei, L.Y.; Wang, M.; Liu, C.J.; Gao, F.; Liang, G.B.; Shao, J.K.; et al. Age and Provenance of Upper Shilidun Formation, Lintan, West Qinling Orogen:Constraints from LA-ICP-MS U-Pb Dating of Detrital Zircons. *Earth Sci.* **2019**, *44*, 1389–1405. (In Chinese with English Abstract)

Disclaimer/Publisher's Note: The statements, opinions and data contained in all publications are solely those of the individual author(s) and contributor(s) and not of MDPI and/or the editor(s). MDPI and/or the editor(s) disclaim responsibility for any injury to people or property resulting from any ideas, methods, instructions or products referred to in the content.